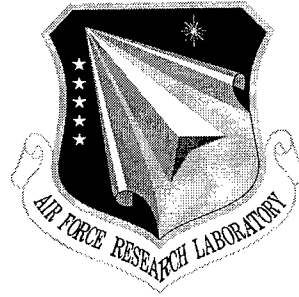


**AFRL-SN-RS-TR-1998-27**

**Final Technical Report**

**March 1998**



## **IMPROVED WSBI INVERSION FOR ROTH**

**Research Associates for Defense Conversion**

**Sergey V. Fridman**

*APPROVED FOR PUBLIC RELEASE; DISTRIBUTION UNLIMITED.*

**DTIC QUALITY INSPECTED 4**

**AIR FORCE RESEARCH LABORATORY  
SENSORS DIRECTORATE  
ROME RESEARCH SITE  
ROME, NEW YORK**

**19980505 062**

This report has been reviewed by the Air Force Research Laboratory, Information Directorate, Public Affairs Office (IFOIPA) and is releasable to the National Technical Information Service (NTIS). At NTIS it will be releasable to the general public, including foreign nations.

AFRL-SN-RS-TR-1998-27 has been reviewed and is approved for publication.

APPROVED:

*FRANK T. BERKEY*

FRANK T. BERKEY  
Project Engineer

FOR THE DIRECTOR:

*Robert G. Polce*

ROBERT G. POLCE, Acting Chief  
Rome Operations Office  
Sensors Directorate

If your address has changed or if you wish to be removed from the Air Force Research Laboratory Rome Research Site mailing list, or if the addressee is no longer employed by your organization, please notify AFRL/SNRD, 26 Electronic Parkway, Rome, NY 13441-4514. This will assist us in maintaining a current mailing list.

Do not return copies of this report unless contractual obligations or notices on a specific document require that it be returned.

REPORT DOCUMENTATION PAGE			Form Approved OMB No. 0704-0188	
Public reporting burden for this collection of information is estimated to average 1 hour per response, including the time for reviewing instructions, searching existing data sources, gathering and maintaining the data needed, and completing and reviewing the collection of information. Send comments regarding this burden estimate or any other aspect of this collection of information, including suggestions for reducing this burden, to Washington Headquarters Services, Directorate for Information Operations and Reports, 1215 Jefferson Davis Highway, Suite 1204, Arlington, VA 22202-4302, and to the Office of Management and Budget, Paperwork Reduction Project (0704-0188), Washington, DC 20503.				
1. AGENCY USE ONLY (Leave blank)	2. REPORT DATE March 1998	3. REPORT TYPE AND DATES COVERED Final Aug 96 - Aug 97		
4. TITLE AND SUBTITLE  IMPROVED WSBI INVERSION FOR ROTH		5. FUNDING NUMBERS c - F30602-96-C-0292 PE - 31315F PR - 4211 TA - 00 WU - P3		
6. AUTHOR(S)  Sergey V. Fridman		8. PERFORMING ORGANIZATION REPORT NUMBER  N/A		
7. PERFORMING ORGANIZATION NAME(S) AND ADDRESS(ES) Prime Contractor Research Associates for Defense Conversion 10002 Hillside Terrace Marcy NY 13405  Sub Contractor: Fridman Associates 2746 Virginia Colony Drive Webster TX 77598		9. SPONSORING/MONITORING AGENCY NAME(S) AND ADDRESS(ES)  Air Force Research Laboratory/SNRD 26 Electronic Parkway Rome NY 13441-4514		
9. SPONSORING/MONITORING AGENCY NAME(S) AND ADDRESS(ES)  Air Force Research Laboratory/SNRD 26 Electronic Parkway Rome NY 13441-4514		10. SPONSORING/MONITORING AGENCY REPORT NUMBER  AFL-SN-RS-TR-1998-27		
11. SUPPLEMENTARY NOTES  Air Force Research Laboratory Project Engineer: Frank T. Berkey/SNRD/(315) 330-4516				
12a. DISTRIBUTION AVAILABILITY STATEMENT  Approved for public release; distribution unlimited.		12b. DISTRIBUTION CODE		
13. ABSTRACT (Maximum 200 words) Wide sweep backscatter ionograms (WSBI) and quasi vertical incidence (QVI) ionograms are routinely collected at over-the-horizon radar (OTHR) installations operated by the U.S. Navy. The WSBI provides information about ionospheric regions that are far down range from the sounder. In this project a method for the quantitative extraction of this information by means of a leading edge inversion technique is described and applied to data acquired by the WSBI sounder operating at the Chesapeake VA OTHR facility. Because this sounder is used to sample 8 azimuthal sections, maps of plasma frequency at a constant altitude can be derived over a geographic region that covers a 64 - 80 degree angular sector out to distances of more than 2000 km. In this report we illustrate the unique capability of the OTHR WSBI sounders to provide real-time monitoring of the ionosphere over a large geographical area.				
14. SUBJECT TERMS  Over-The-Horizon Radar, Electron Density Profiles, Electromagnetic Radiation, Ionospheric Propagation		15. NUMBER OF PAGES 76		
17. SECURITY CLASSIFICATION OF REPORT  UNCLASSIFIED		18. SECURITY CLASSIFICATION OF THIS PAGE  UNCLASSIFIED		16. PRICE CODE
17. SECURITY CLASSIFICATION OF REPORT  UNCLASSIFIED		18. SECURITY CLASSIFICATION OF THIS PAGE  UNCLASSIFIED		19. SECURITY CLASSIFICATION OF ABSTRACT  UNCLASSIFIED
17. SECURITY CLASSIFICATION OF REPORT  UNCLASSIFIED		18. SECURITY CLASSIFICATION OF THIS PAGE  UNCLASSIFIED		20. LIMITATION OF ABSTRACT  UL

## Table of Contents

<b>Introduction</b>	<b>1</b>
<b>1 Theory of WSBI Inversion</b>	<b>3</b>
1.1 Starting Principles .....	3
1.2 Theory and Algorithm for Calculation for the Linearized Group Path Operator .....	7
1.3 WSBI Inversion Using Newton-Kontorovich Method and Tikhonov's Regularization Method .....	17
<b>2 Numerical Solution of Two Dimensional Fredholm Integral Equation of the     First Kind</b>	<b>22</b>
2.1 General Relationships.....	22
2.2 Regularization Method in a Rectangular Region .....	25
2.3 Numerical Realization of the Rectangulization Method for Two-Dimensional Integral Equation of the First Kind.....	26
<b>3 Reconstruction of the Ionosphere from WSBI Data Collected by the Virginia     OTHR</b>	<b>32</b>
<b>4 Discussion and Conclusion</b>	<b>47</b>
<b>References</b>	<b>51</b>

## List of Figures

1a	Fitting the Leading Edge data in the 8 Channels: Channels 1-4.....	33
1b	Fitting the Leading Edge data in the 8 Channels: Channels 5-8.....	34
2	3-D Inversion of WSBI Leading Edge: plasma frequency (MHz) at h = 235km .....	36
3a	Fitting the Leading Edge data in the 8 Channels: Channels 1-4.....	38
3b	Fitting the Leading Edge data in the 8 Channels: Channels 5-8.....	39
4	3-D Inversion of WSBI Leading Edge: plasma frequency (MHz) at h = 247km .....	40
5	3-D Inversion of WSBI Leading Edge: plasma frequency (MHz) at h = 260km .....	41
6a	Fitting the Leading Edge data in the 8 Channels: Channels 1-4.....	42
6b	Fitting the Leading Edge data in the 8 Channels: Channels 5-8.....	43
7	3-D Inversion of WSBI Leading Edge: plasma frequency (MHz) at h = 243km .....	44
8	3-D Inversion of WSBI Leading Edge: plasma frequency (MHz) at h = 243km .....	45
9	3-D Inversion of WSBI Leading Edge: plasma frequency (MHz) at h = 243km .....	46
10	3-D Inversion of WSBI Leading Edge: plasma frequency (MHz) at h = 243km .....	48

11 3-D Inversion of WSBI Leading Edge: plasma frequency (MHz) at

h = 243km .....49

## Introduction

To facilitate the OTHR coordinate registration process, bistatic backscatter sounders are routinely operated along with QVI sounders at the two operational facilities in Virginia and Texas [Headrick, 1990; Headrick and Skolnik, 1974]. These sounders have azimuthal receive antenna beam steering capability, so that a BI can be measured for a set of beam directions within the azimuthal coverage sector of each backscatter sounder. Here, we combine each of the eight individual WSBI s obtained at different azimuths to form an integrated view of the ionospheric density over the OTHR coverage sector ( $64^{\circ}$ - $80^{\circ}$ ).

Each WSBI typically has a distinct leading edge which is, to first order, independent of the scattering properties of Earth's surface and, in the case of a narrow antenna beam, is determined entirely by the three-dimensional distribution of electron density existing in the ionosphere. The theoretical leading edge for a specific ionospheric model may be found to high accuracy by using ray tracing, as discussed in Section 2.

The leading edge of the WSBI contains information about ionospheric regions located thousands of kilometers away from the sounder and the inverse problem of backscatter sounding, as we address it here, is the problem of extraction of the plasma density distribution in the ionosphere from the measured leading edge. This inverse problem is rather cumbersome, because even the solution of the direct problem (the relationship between the plasma density distribution and the leading edge) can not be expressed explicitly. A rigorous approach that addresses the numerical solution of this problem was developed recently by *Fridman and Fridman* [1994]. This approach is

based on the Newton-Kontorovich method for the solution of nonlinear operator equations and on Tikhonov's regularization method for ill-posed problems. *Fridman and Fridman* [1994] considered the inverse problem for a single WSBI and reconstructed the two-dimensional electron density distribution in a vertical plane aligned in the direction of sounding. The technique was found to accurately reconstruct the ionosphere in numerous tests, both against simulated data as well as multi-station experimental data [*Fridman et al.*, 1994].

In this project, the approach of *Fridman and Fridman* [1994] is extended to develop a method for the reconstruction of the three-dimensional ionosphere from the OTHR WSBI data. A regularized formulation of the WSBI inversion problem and specific numerical methods for this nonlinear inverse problem are described in Section 1. The key element for the solution of nonlinear problem is Tikhonov's method for two-dimensional linear problems developed in Section 2. Section 3 presents several examples of inversions for data collected by the OTHR located near Chesapeake, VA. In conclusion, the WSBI inversion technique is discussed as a new method for ionospheric diagnostics.

## 1. Theory of WSBI Inversion

### 1.1 Starting Principles

The measured WSBI leading edge is a function of two variables  $\tilde{g}(f, \varphi)$  because it represents the dependence of the minimal group delay on frequency  $f$  and azimuth  $\varphi$ . The theoretical value of this function  $g(f, \varphi)$ , for any given distribution of electron density  $n(x_1, x_2, x_3)$  specified in a system of coordinates  $x_1, x_2, x_3$ , may be calculated by numerical solution of the ray tracing equations as follows: for each frequency and each azimuthal beam, a fan of oblique rays exiting in the central azimuthal direction of the beam at different elevation angles is considered, and the ray that exhibits the minimal group delay for propagation from the sounder to a point of first contact with the Earth and back to the sounder is derived. This minimal group delay and the current value of operating frequency represent two coordinates of a point in the leading edge plot. Every point of the leading edge is obtained by applying the above procedure to the full set of operating frequencies (the frequency range is 5-28 MHz for the Virginia OTHR). Formally, this process establishes a nonlinear operator  $\hat{G}_n$  that transforms  $n(x_1, x_2, x_3)$  into  $g(f, \varphi)$ . It can be represented symbolically as

$$g = \hat{G}_n n. \quad (1)$$

Essentially, WSBI inversion may be viewed as resolving this equation with respect to  $n$ . The equation is obviously underdetermined because the known function  $\tilde{g}$  is a function of two variables, whereas the function to be found depends on three variables. In order to avoid this inconsistency, we parameterize  $n$  by a function of two variables that is denoted

as  $u(s_1, s_2)$ . The physical meaning of  $u$  and of the variables  $s_1, s_2$  depends on the selected form of the parametrization. The most general parametrization may be formally represented as

$$n = \hat{N}u \quad (2)$$

where  $\hat{N}$  is a known operator (generally nonlinear) that transforms  $u$  into  $n$ . The method described below is designed to work with an arbitrary parametrization, however in all the examples presented in this report, we use the following simple form of parameterization

$$n(x_1, x_2, x_3) = n_0(x_3)[1 + u(x_1, x_2)], \quad (3)$$

where  $n_0(x_3)$  is the vertical profile of electron density as measured by the QVI sounder at the OTHR site. Here and below we require that coordinates  $x_1, x_2$  specify the geographic position of a point and the altitude is determined by  $x_3$ .

After the parametrization is introduced we have  $g = \hat{G}_u u$ , where  $\hat{G}_u = \hat{G}_n \hat{N}$  defines the group path operator. The inverse problem is the task of resolving the functional equation

$$\tilde{g} = \hat{G}_u u, \quad (4)$$

where  $u$  is the unknown function in this equation.

Inverse problems such as the one considered here are usually unstable [Tikhonov and Arsenin, 1977], meaning that even the smallest error of measurement in  $\tilde{g}$  causes considerable deviation of the solution  $u$  from the true solution. In order to stabilize the solution we have incorporated Tikhonov's method of regularization [Tikhonov and Arsenin, 1977] in this work. The essence of this method, as applied to the WSBI inversion problem may be formulated as follows: All possible functions  $u$  that satisfy

equation (4) within the accuracy of measurement of the leading edge  $\tilde{g}$  are considered, and among these functions the smoothest one is chosen as the optimal solution.

In order to implement this approach, a quantitative measure of the smoothness of  $u$  must be introduced. This measure is called the stabilizing functional  $\Omega[u]$  and is defined by

$$\Omega[u] = \iint \left[ u^2 + q_1 \left( \frac{\partial u}{\partial s_1} \right)^2 + q_2 \left( \frac{\partial u}{\partial s_2} \right)^2 \right] w ds_1 ds_2, \quad (5)$$

where  $q_1(s_1, s_2)$ ,  $q_2(s_1, s_2)$ , and  $w(s_1, s_2)$  are arbitrary positive weight functions that are chosen in accordance with the symmetry of the system of coordinates and the typical scales of the task in consideration. Let  $\delta$  be an *a priori* root-mean-square error of measurement of the WSBI leading edge, then the regularized solution of the inverse problem obeys the following relationships:

$$\int_{\varphi_{\min}}^{\varphi_{\max}} \int_{f_{\min}}^{f_{\max}} (\tilde{g} - \hat{G}_u u)^2 d\varphi df \leq \delta^2 (\varphi_{\max} - \varphi_{\min}) (f_{\max} - f_{\min}) \quad (6)$$

$$\Omega[u] \rightarrow \min \quad (7)$$

where  $\varphi_{\max}$ ,  $\varphi_{\min}$  and  $f_{\max}$ ,  $f_{\min}$  are respectively, the upper and lower bounds of the azimuthal direction and frequency of the transmitted sounder beam pattern. Thus, the functional  $\Omega[u]$  is minimized on all  $u$  that satisfy the inequality (6).

A procedure for the numerical solution of the problem stated by (6) and (7) has been developed as a generalization to three dimensions of the technique for BI inversion in two dimensions described in *Fridman and Fridman* [1994]. It is an iterative process, where each iteration executes the following three steps:

1. Ray tracing synthesis of the WSBI leading edge for a given ionospheric model,
2. Linearization of the operator  $\hat{G}_u$  (based on the solution of the linearized ray tracing equations),
3. Calculation of corrections to the ionospheric model by solving the problem stated by (4) and (5) with  $\hat{G}_u$  replaced by its linearized approximation. The solution is attained by applying the regularization method for linear problems, a method developed originally by *Tikhonov and Arsenin* [1977].

The corrected model obtained from step 3 is used in the next iteration for step 1. The iterations are continued until the model converges.

Input data for the inversion procedure include: (i) a table of WSBI leading edge  $\tilde{g}(f, \varphi)$ ; (ii) the *a priori* root-mean-square error  $\delta$  of the leading edge measurement; (iii) the overhead vertical profile  $n_0(h)$  obtained from the QVI data ( $h$  is altitude). The output is a three-dimensional distribution of electron density for the area covered by the sounder. The maximum height attained by this inversion is always below the F2 region ionospheric maximum, because all rays forming the leading edge are refracted below the peak of electron density.

In this report we will describe the most important developments of the inversion technique achieved during the course of this project. In 1.2 we will describe the theory and algorithm for calculation of the linearized group path operator. Then, in 1.3, our realization of the Tikhonov's regularization method for the nonlinear problem in consideration is presented.

## 1.2 Theory and Algorithm for Calculation of the Linearized Group Path Operator

Let us denote as  $\bar{P}(\beta, \varphi, f)$  the group path from the transmitter to the point of the first contact with the Earth for a ray exiting the transmitter at the elevation angle  $\beta$  (measured from the vertical direction), azimuth  $\varphi$ , and operating frequency  $f$ . Available ray-tracing codes are able to perform accurate calculations of this function. The leading edge

$g(f, \varphi)$  is related to the function  $P$  as follows:

$$g(f, \varphi) = \min_{0 < \beta < \pi/2} \bar{P}(\beta, \varphi, f) \quad (8)$$

The elevation angle at which the group path  $P$  is a minimum we will denote as  $\beta_m(\varphi, f)$ .

So that

$$g(f, \varphi) = \bar{P}[\beta_m(\varphi, f), \varphi, f] \quad (9)$$

Consider variations of functions  $\bar{P}$ ,  $\beta_m$ , and  $g$  associated with an infinitesimal variation  $\delta n$  of electron density in the ionosphere. That is suppose that

$$n(x_1, x_2, x_3) = n_0(x_1, x_2, x_3) + \delta n(x_1, x_2, x_3)$$

$$\bar{P}(\beta, \varphi, f) = \bar{P}_0(\beta, \varphi, f) + \delta \bar{P}(\beta, \varphi, f)$$

$$\beta_m(\varphi, f) = \beta_{m0}(\varphi, f) + \delta \beta_m(\varphi, f)$$

$$g(f, \varphi) = g_0(f, \varphi) + \delta g(f, \varphi)$$

Variation of the leading edge  $\delta g$  may be expressed in terms of  $\delta \bar{P}$  and  $\delta \beta_m$ . From (9)

we have:  $\delta g(f, \varphi) = \delta \bar{P}(\beta_{m0}, \varphi, f) + \delta \beta_m(\varphi, f) \partial \bar{P}_0(\beta_{m0}, \varphi, f) / \partial \beta$ . The second term in the right-hand side is equal to zero because of (8), so that

$$\delta g(f, \varphi) = \delta \bar{P}(\beta_{m0}, \varphi, f) \quad (10)$$

In order to proceed further we will need to use a concrete system of ray tracing equations. However the results obtained may be easily generalized for any arbitrary form of ray-tracing equations.

To simplify the procedure and to reduce the computation time, we neglect azimuthal displacements acquired by the rays during their propagation in the ionosphere. This approximation is justified by the fact that in the first approximation these displacements do not affect the leading edge. Effects of the geomagnetic field will be also neglected. With these simplifications the ray tracing equations may be represented in the form:

$$\begin{aligned} \frac{dy_1}{dx} &= F_1(x, y_1, y_2) \\ \frac{dy_2}{dx} &= F_2(x, y_1, y_2) \\ \frac{dy_3}{dx} &= F_3(x, y_1, y_2) \end{aligned} \quad (11)$$

where

$$F_1(x, y_1, y_2) = \frac{y_2}{\sqrt{\tilde{\epsilon} - y_2^2}} \quad (12)$$

$$F_2(x, y_1, y_2) = \frac{1}{2\sqrt{\tilde{\epsilon} - y_2^2}} \frac{\partial}{\partial z} \tilde{\epsilon} \quad (13)$$

$$F_3(x, y_1, y_2) = \frac{\exp(2y_1 / R_E)}{\sqrt{\tilde{\epsilon} - y_2^2}} \quad (14)$$

$$y_1 = R_E \log(1 + h / R_E) \quad (15)$$

$$y_2 = \sqrt{\tilde{\epsilon}} \cos \beta \quad (16)$$

$$y_3 = P' \quad (17)$$

$$z = R_E \log(1 + h / R_E) \quad (18)$$

$$\tilde{\epsilon} = (1 + h / R_E)^2 \epsilon \quad (19)$$

$$\epsilon = 1 - \frac{f_p^2}{f^2} \quad (20)$$

$$f_p = \sqrt{\frac{ne^2}{\pi m}} \quad (21)$$

$P'$  is the current value of the group path, and  $x$  is the range along the earth surface measured in the direction of the exit azimuth.

Let us write down linearized equations (11) by substituting in (11)-(20) the following expressions

$$y_1 = y_{10} + \delta y_1$$

$$y_2 = y_{20} + \delta y_2$$

$$y_3 = y_{30} + \delta y_3$$

$$f_p^2 = f_{p0}^2 + \delta f_p^2$$

and implying that  $y_{10}, y_{20}, y_{30}$ , and  $f_{p0}^2$  satisfy to (11). As a result the following system

of equations may be obtained:

$$\frac{d}{dx} \begin{bmatrix} \delta y_1 \\ \delta y_2 \\ \delta y_3 \end{bmatrix} + \begin{bmatrix} a_{11} & a_{12} & 0 \\ a_{21} & a_{22} & 0 \\ a_{31} & a_{32} & 0 \end{bmatrix} \begin{bmatrix} \delta y_1 \\ \delta y_2 \\ \delta y_3 \end{bmatrix} = \begin{bmatrix} b_1 \\ b_2 \\ b_3 \end{bmatrix} \delta f_p^2 + \begin{bmatrix} 0 \\ c_2 \\ 0 \end{bmatrix} \frac{\partial}{\partial h} \delta f_p^2 \quad (22)$$

where

$$a_{11}(x) = \frac{y_{20}}{2(\tilde{\epsilon}_0 - y_{20}^2)^{3/2}} \frac{\partial}{\partial z} \tilde{\epsilon}_0; \quad (23)$$

$$a_{12}(x) = -\frac{\tilde{\epsilon}_0}{(\tilde{\epsilon}_0 - y_{20}^2)^{3/2}}, \quad (24)$$

$$a_{21}(x) = -\frac{1}{2\sqrt{\tilde{\epsilon}_0 - y_{20}^2}} \frac{\partial^2 \tilde{\epsilon}_0}{\partial z^2} + \frac{1}{4(\tilde{\epsilon}_0 - y_{20}^2)^{3/2}} \left( \frac{\partial \tilde{\epsilon}_0}{\partial z} \right)^2, \quad (25)$$

$$a_{22}(x) = -\frac{y_{20}}{2(\tilde{\epsilon}_0 - y_{20}^2)^{3/2}} \frac{\partial \tilde{\epsilon}_0}{\partial z}, \quad (26)$$

$$a_{31}(x) = -\frac{\exp(2y_{10}/R_E)}{2\sqrt{\tilde{\epsilon}_0 - y_{20}^2}} \left( \frac{4}{R_E} - \frac{1}{\tilde{\epsilon}_0 - y_{20}^2} \frac{\partial \tilde{\epsilon}_0}{\partial z} \right), \quad (27)$$

$$a_{32}(x) = -\frac{\exp(2y_{10}/R_E) y_{20}}{(\tilde{\epsilon}_0 - y_{20}^2)^{3/2}}, \quad (28)$$

$$b_1 = \frac{y_{20} \exp(2y_{10}/R_E)}{2f^2 (\tilde{\epsilon}_0 - y_{20}^2)^{3/2}}, \quad (29)$$

$$b_2 = -\frac{\exp(2y_{10}/R_E)}{2f^2} \left[ \frac{2}{R_E \sqrt{\tilde{\epsilon}_0 - y_{20}^2}} - \frac{1}{2(\tilde{\epsilon}_0 - y_{20}^2)^{3/2}} \frac{\partial}{\partial z} \tilde{\epsilon}_0 \right], \quad (30)$$

$$b_3 = \frac{\exp(2y_{10}/R_E)}{2f^2 (\tilde{\epsilon}_0 - y_{20}^2)^{3/2}}, \quad (31)$$

$$c_2 = -\frac{\exp(3y_{10}/R_E)}{2f^2 \sqrt{\tilde{\epsilon}_0 - y_{20}^2}}. \quad (32)$$

For our purpose equation (22) should be considered with zero initial conditions. The nearest goal is to find the relationship between  $\delta g$  and  $\delta f_p$  that follows from (22).

Suppose that the value of  $\beta_{m0}$  for an unperturbed ionosphere is found. Then we take the solution that corresponds to the exit angle  $\beta_{m0}$  as the zeroth order solution to be used in (22). Suppose that equation (22) is solved for a given  $\delta f_p$ , then according to (10)

$$\begin{aligned}\delta g &= \delta \bar{P}(\beta_{m0}) = y_3(\bar{x}_{m0} + \delta \bar{x}_m) - y_{30}(\bar{x}_{m0}) = \delta \bar{x}_m \frac{d}{dx} y_{30}(\bar{x}_{m0}) + \delta y_3(\bar{x}_{m0}) \\ &= - \frac{\delta y_1(\bar{x}_{m0})}{dy_{10}(\bar{x}_{m0})/dx} \frac{d}{dx} y_{30}(\bar{x}_{m0}) + \delta y_3(\bar{x}_{m0})\end{aligned}$$

So that

$$\begin{aligned}\delta g &= \delta \bar{P}(\beta_{m0}) = \delta y_3(\bar{x}_{m0}) - \frac{F_{30}[\bar{x}_{m0}, 0, y_2(\bar{x}_{m0})]}{F_{10}[\bar{x}_{m0}, 0, y_2(\bar{x}_{m0})]} \delta y_1(\bar{x}_{m0}) = \\ &\delta y_3(\bar{x}_{m0}) - \frac{1}{\cos \beta_0} \delta y_1(\bar{x}_{m0})\end{aligned}\tag{33}$$

Here  $\bar{x}_m$  denotes the value of  $x$  for the first landing point of the ray, and  $\bar{\beta}$  is the elevation angle at arrival in the landing point,  $F_{10}$  and  $F_{30}$  are correspondingly  $F_1$  and  $F_3$  for the unperturbed ionosphere.

Now it is convenient to introduce Green's function for equation (22) (or unit impulse response function). Namely we introduce a 3 by 3 matrix  $\mathbf{R}(x, x')$  that satisfies the equation:

$$\frac{d}{dx} \mathbf{R} + \mathbf{a} \mathbf{R} = \mathbf{I} \delta(x - x')$$

with zero initial conditions ( $\mathbf{R}(x, x') = 0$  at  $x < x'$ ). Here  $\mathbf{I}$  is a unit 3 by 3 matrix, and

$$\mathbf{a} = \begin{bmatrix} a_{11} & a_{12} & 0 \\ a_{21} & a_{22} & 0 \\ a_{31} & a_{32} & 0 \end{bmatrix}.$$

The variation of the leading edge may be written as

$$\delta g = \int_0^{\bar{x}_{m0}} \left\{ G'(x') \delta f_p^2 [x_1(x'), x_2(x'), x_3(x')] + G''(x') \frac{\partial}{\partial h} \delta f_p^2 [x_1(x'), x_2(x'), x_3(x')] \right\} dx' \quad (34)$$

where the functions  $x_1(x'), x_2(x'), x_3(x')$  are specifying the ray's trajectory, and

$$\begin{aligned} G'(x') &= \sum_{n=1}^3 \left\{ R_{3n}(\bar{x}_{m0}, x') - \frac{F_{30}[\bar{x}_{m0}, 0, y_2(\bar{x}_{m0})]}{F_{10}[\bar{x}_{m0}, 0, y_2(\bar{x}_{m0})]} R_{1n}(\bar{x}_{m0}, x') \right\} b_n(x') \\ G''(x') &= \sum_{n=1}^3 \left\{ R_{3n}(\bar{x}_{m0}, x') - \frac{F_{30}[\bar{x}_{m0}, 0, y_2(\bar{x}_{m0})]}{F_{10}[\bar{x}_{m0}, 0, y_2(\bar{x}_{m0})]} R_{1n}(\bar{x}_{m0}, x') \right\} c_n(x') = \\ &\quad \left[ R_{32}(\bar{x}_{m0}, x') - \frac{1}{\cos \beta_0} R_{12}(\bar{x}_{m0}, x') \right] c_2(x') \end{aligned} \quad (35)$$

The unit impulse response may be expressed in terms of three linearly independent solutions of (22) with  $\delta f_p^2 = 0$ . We obtain such solutions  $\mathbf{e}_1(x), \mathbf{e}_2(x), \mathbf{e}_3(x)$  by solving uniform equation (22) for three instances of initial conditions:

$$\mathbf{e}_1(0) = \begin{bmatrix} 1 \\ 0 \\ 0 \end{bmatrix}; \mathbf{e}_2(0) = \begin{bmatrix} 0 \\ 1 \\ 0 \end{bmatrix}; \mathbf{e}_3(0) = \begin{bmatrix} 0 \\ 0 \\ 1 \end{bmatrix}.$$

Then,

$$\mathbf{R}(x, x') = \mathbf{E}(x) \mathbf{E}^{-1}(x') \theta(x - x') \quad (35)$$

Here matrix  $\mathbf{E}$  consists of columns  $\mathbf{e}_1(x), \mathbf{e}_2(x), \mathbf{e}_3(x)$ :

$$\mathbf{E}(x) = [\mathbf{e}_1(x), \mathbf{e}_2(x), \mathbf{e}_3(x)];$$

and  $\theta(x)$  is the unit step function ( $\theta(x) = 0$  at  $x < 0$  and  $\theta(x) = 1$  at  $x > 0$ ).

Calculation of the inverse matrix is simplified by the fact that

$$\mathbf{e}_3(x) = \begin{bmatrix} 0 \\ 0 \\ 1 \end{bmatrix} \text{ so that } \mathbf{E}(x) = \begin{bmatrix} e_{11}(x) & e_{21}(x) & 0 \\ e_{12}(x) & e_{22}(x) & 0 \\ e_{13}(x) & e_{23}(x) & 1 \end{bmatrix} \text{ and}$$

$$\mathbf{E}^{-1}(x) = \frac{1}{e_{22}e_{11} - e_{21}e_{12}} \begin{bmatrix} e_{22} & -e_{21} & 0 \\ -e_{12} & e_{11} & 0 \\ -e_{22}e_{13} + e_{21}e_{23} & e_{13}e_{21} - e_{23}e_{11} & 1 \end{bmatrix} \quad (36)$$

The components of  $\mathbf{R}$  involved in the expression (34) for leading edge response are:

$$R_{11}(\bar{x}_{m0}, x') = \frac{e_{11}(\bar{x}_{m0})e_{22}(x') - e_{21}(\bar{x}_{m0})e_{12}(x')}{e_{22}(x')e_{11}(x') - e_{21}(x')e_{12}(x')} \quad (37)$$

$$R_{12}(\bar{x}_{m0}, x') = \frac{-e_{11}(\bar{x}_{m0})e_{21}(x') + e_{21}(\bar{x}_{m0})e_{11}(x')}{e_{22}(x')e_{11}(x') - e_{21}(x')e_{12}(x')} \quad (38)$$

$$R_{13}(x, x') = 0 \quad (39)$$

$$R_{31}(\bar{x}_{m0}, x') = \frac{e_{13}(\bar{x}_{m0})e_{22}(x') - e_{23}(\bar{x}_{m0})e_{12}(x') - e_{22}(x')e_{13}(x') + e_{21}(x')e_{23}(x')}{e_{22}(x')e_{11}(x') - e_{21}(x')e_{12}(x')} \quad (40)$$

$$R_{32}(\bar{x}_{m0}, x') = \frac{-e_{13}(\bar{x}_{m0})e_{21}(x') + e_{23}(\bar{x}_{m0})e_{11}(x') + e_{21}(x')e_{13}(x') - e_{11}(x')e_{23}(x')}{e_{22}(x')e_{11}(x') - e_{21}(x')e_{12}(x')} \quad (41)$$

$$R_{33}(\bar{x}_{m0}, x') = 1. \quad (42)$$

Let us approximate integrals and derivatives in (34) by finite sums and differences.

Denoting as  $w_l$  the coefficients the integration formula we obtain:

$$\delta g = \sum_l \left\{ G'(x'_l) \delta f_p^2 [x_1(x'_l), x_2(x'_l), h(x'_l)] + G''(x'_l) \frac{\partial}{\partial h} \delta f_p^2 [x_1(x'_l), x_2(x'_l), h(x'_l)] \right\} w_l =$$

$$\sum_l w_l \left\{ G'(x'_l) \delta f_p^2 [x_1(x'_l), x_2(x'_l), h(x'_l)] + \right.$$

$$\left. G''(x'_l) \frac{\delta f_p^2 [x_1(x'_l), x_2(x'_l), h_{k_0(l)+1}] - f_p^2 [x_1(x'_l), x_2(x'_l), h_{k_0(l)}]}{h_{k_0(l)+1} - h_{k_0(l)}} \right\} \quad (43)$$

Furthermore, by invoking interpolation the above expression may be approximately represented as:

$$\delta g = \sum_{i,j,k} G_{ijk} \delta f_p^2(i, j, k), \quad (45)$$

where integer variables  $i, j$ , and  $k$  denote the nodes of a 3-D spatial grid in which the 3-D ionosphere is specified. Using triple linear interpolation we obtain the following expressions for nonzero elements of the matrix  $G$ :

$$G_{ijk} = \sum_{l: i_0(l)=i \& j_0(l)=j \& k_0(l)=k} \left[ G'_l (1 - p_3(l)) - G''_l \frac{1}{h_{k+1} - h_k} \right] (1 - p_1(l)) (1 - p_2(l)) w_l$$

$$+ \sum_{l: i_0(l)+1=i \& j_0(l)=j \& k_0(l)=k} \left[ G'_l (1 - p_3(l)) - G''_l \frac{1}{h_{k+1} - h_k} \right] p_1(l) (1 - p_2(l)) w_l$$

$$+ \sum_{l: i_0(l)=i \& j_0(l)+1=j \& k_0(l)=k} \left[ G'_l (1 - p_3(l)) - G''_l \frac{1}{h_{k+1} - h_k} \right] (1 - p_1(l)) p_2(l) w_l$$

$$+ \sum_{l: i_0(l)=i \& j_0(l)=j \& k_0(l)+1=k} \left[ G'_l p_3(l) + G''_l \frac{1}{h_k - h_{k-1}} \right] (1 - p_1(l)) (1 - p_2(l)) w_l$$

$$+ \sum_{l: i_0(l)=i \& j_0(l)+1=j \& k_0(l)+1=k} \left[ G'_l p_3(l) + G''_l \frac{1}{h_k - h_{k-1}} \right] (1 - p_1(l)) p_2(l) w_l$$

$$\begin{aligned}
& + \sum_{l: i_0(l)+1=i \& j_0(l)=j \& k_0(l)+1=k} \left[ G'_l p_3(l) + G''_l \frac{1}{h_k - h_{k-1}} \right] p_1(l) (1 - p_2(l)) w_l \\
& + \sum_{l: i_0(l)+1=i \& j_0(l)+1=j \& k_0(l)=k} \left[ G'_l (1 - p_3(l)) - G''_l \frac{1}{h_{k+1} - h_k} \right] p_1(l) p_2(l) w_l \\
& + \sum_{l: i_0(l)+1=i \& j_0(l)+1=j \& k_0(l)+1=k} \left[ G'_l p_3(l) + G''_l \frac{1}{h_k - h_{k-1}} \right] p_1(l) p_2(l) w_l
\end{aligned} \tag{46}$$

The following functions has been introduced above:

$$\begin{aligned}
i_0(l): x_1(l) < x_1^{i_{\min}} & \Rightarrow i_0 = i_{\min} \\
x_1(l) \geq x_1^{i_{\max}} & \Rightarrow i_0 = i_{\max} - 1 \\
x_1^{i_{\min}} \leq x_1(l) < x_1^{i_{\max}} & \Rightarrow i_0 = \max i_0: x_1^{i_0} \leq x_1(l)
\end{aligned} \tag{47}$$

$$p_1(l) = \frac{x_1(l) - x_1^{i_0(l)}}{x_1^{i_0(l)+1} - x_1^{i_0(l)}} \tag{48}$$

The pairs of functions  $j_0(l), p_2(l)$  and  $k_0(l), p_2(l)$  are defined in a similar way for spatial variables  $x_2$  and  $x_3 = h$ , correspondingly. Notations  $x_1^i, x_2^j, x_3^k = h_k$  are introduced for nodes of the variables  $x_1, x_2, x_3$ .

When realizing these formula it is convenient to have the variables  $x_1$  and  $x'$  to be the same. Then each sum in (46) contains only one element and the second sum is equal to zero. This also permits an economical storage of the array G. Its nonzero elements may be specified as  $G_{i_0(l), j_0(l), k_0(l)}, G_{i_0(l), j_0(l)+1, k_0(l)}, G_{i_0(l), j_0(l), k_0(l)+1}, G_{i_0(l), j_0(l)+1, k_0(l)+1}$  and can be stored in four vectors of length  $i_{\max} - i_{\min} + 1$ .

Now consider the parametrization of  $f_p^2$  by a function of two variables  $u(s, t)$ .

Linearized relationship (2) may be represented in the form:

$$\delta f_p^2(x_1, x_2, x_3) = \iint \Phi(x_1, x_2, x_3, s, t) \delta u(s, t) ds dt \quad (49)$$

We approximate the above integral by a finite sum with weight coefficients  $r_{mn}$ :

$$\delta f_p^2(i, j, k) = \sum_m \sum_n \Phi(i, j, k, s_m, t_n) \delta u(m, n) r_{mn}. \quad (50)$$

Example. In the case of parametrization (3)

$$\Phi(x_1, x_2, x_3, s, t) = f_{p0}^2(h) \delta(x_1 - s) \delta(x_2 - t)$$

and the finite difference approximation of the above expression is

$$\Phi(i, j, k, s_m, t_n) = f_{p0}^2(h_k) \delta_{im} \delta_{jn} / r_{ij}$$

Using (50) in (45) obtain:

$$\delta g = \sum_m \sum_n K'(m, n) r_{mn} \delta u(m, n) \quad (51)$$

where

$$K'(m, n) = \sum_i \sum_j \sum_k G_{ijk} \Phi(i, j, k, s_m, t_n) \quad (52)$$

Note that (51) is a finite sum approximation for the integral

$$\delta g = \iint K'(s, t) \delta u(s, t) ds dt \quad (53)$$

It should be remembered that the function  $K'$  depends also on frequency and the azimuthal direction of sounding.

Relationships (35), (37)-(42), (46)-(48), (52), (51) determine the desired linearized group path operator.

### 1.3 WSBI Inversion Using Newton-Kontorovich Method and Tikhonov's Regularization Method

Input data for the inversion procedure include: (i) a table of WSBI leading edge  $\tilde{g}(f, \varphi)$ ; (ii) the *a priori* root-mean-square error  $\delta$  of the leading edge measurement; (iii) the overhead vertical profile  $n_0(h)$  obtained from the QVI data ( $h$  is altitude), and (iv) the *a priori* root-mean-square error  $\eta$  of the vertical profile.

Our ionospheric model is specified by an unknown function of two variables

$u(s_1, s_2)$  and a known operator  $\hat{N}$ :

$$n(x_1, x_2, h) = \hat{N}u \quad (54)$$

The function must be in agreement with the measured WSBI. It also must be in agreement with  $n_0(h)$ , that is there should be

$$n(x_{10}, x_{20}, h) \approx n_0(h) \quad (55)$$

at the QVI location specified by coordinates  $x_{10}, x_{20}$ . We imply that the operator  $\hat{N}$  is consistent with (55). Thus, the functional equations to be solved are:

$$\hat{G}_u u = \tilde{g} \quad (56)$$

$$\hat{N}_S u = n_0 \quad (57)$$

Here we have introduced the operator  $\hat{N}_S$  that produces the vertical profile at the QVI location:

$$\hat{N}_S u = \hat{N}u|_{x_1=x_{10}, x_2=x_{20}} \quad (58)$$

We are looking for a regularized approximate solution of (56), (57). We define the regularized solution according to the following relationships.

$$(1 - \mu) \frac{\|\hat{G}_u u - \tilde{g}\|^2}{\delta^2} + \mu \frac{\|\hat{N}_S u - n_0\|^2}{\eta^2} \leq 1 \quad (59)$$

$$\Omega[u] \rightarrow \min \quad (60)$$

The norm symbol  $\|\cdot\|$  is used here for rms value of a function:

$$\|g(f, \varphi)\| = \sqrt{\frac{1}{L'} \sum_{l'=1}^{L'} [g(f_{l'}, \varphi_{l'})]^2} \quad (61)$$

$$\|n_0(h)\| = \sqrt{\sum_{l''=1}^{L''} [n_0(h_{l''})]^2 / L''} \quad (62)$$

Expression (59) indicates that we consider (56) and (57) as one equation. Parameter  $\mu$  is a positive constant smaller than 1, it is introduced in order to be able to properly weight these equations. Our typical choice of this parameter is  $\mu = 1 / L'$ , where  $L'$  is the total number of points in all WSBI's.

The functional equations (56) and (57) are generally nonlinear. We solve this system iteratively. In each iteration operators  $\hat{N}_S$  and  $\hat{G}_u$  are approximated by their linearizations. This approach to solution of nonlinear operator equations is known as Newton-Kontorovich method [Kolmogorov and Fomin, 1975].

Linearization of the operator  $\hat{N}$  is specified by a known matrix  $\Phi$  in accordance with (50). Without loosing the generality we may accept that  $u=0$  corresponds to the uniform ionosphere with the profile equal to  $n_0(h)$  everywhere and that

$$\begin{aligned} x_{10} &= 0 \\ x_{20} &= 0 \end{aligned}$$

### Major steps of the iterative solution.

1. The starting approximation to the 3-d model of the ionosphere is formed by assuming

$$n(x_1, x_2, h) = n_0(h) \quad (54)$$

2. Ray tracing is used to calculate the theoretical leading edge  $g(f, \varphi)$  and the optimum elevation angle  $\beta_m(\varphi, f)$  functions for all values of frequency and azimuth at which the experimental leading edge points are specified.

3. The rms discrepancy between the experimental and theoretical leading edges

$$\|g - \tilde{g}\| = \sqrt{\frac{1}{L'} \sum_{l=1}^{L'} [g(f_l, \varphi_l) - \tilde{g}(f_l, \varphi_l)]^2}$$

is calculated. If the condition  $(1 - \mu)\|g - \tilde{g}\| \leq \delta$  is satisfied then the ionosphere specified by (54) gives the optimum solution of the inverse problem. Otherwise the iterative process described below is started with

$$\delta g = \tilde{g} - g$$

$$\delta n_0(h) = 0.$$

4. The linearized group path operator  $K'$  (defined in (52)) is calculated as described in 1.2 using  $\beta_m(\varphi, f)$  and  $n(x_1, x_2, h)$  found on the previous step.

5. The system of linear integral equations

$$\iint K'(f, \varphi, s, t) \delta u(s, t) ds dt = \delta g(f, \varphi)$$

$$\iint \Phi(0, 0, h, s, t) \delta u(s, t) ds dt = \delta n_0(h)$$

is solved numerically using Tikhonov's regularization method described in Chapter 2.

When performing this solution the system is treated as a single integral equation of the form

$$\iint K(l, s, t) \delta u(s, t) ds dt = f_t(l)$$

with the discrete representations of the kernel and the RHS taken as:

$$K(l, i, j) = \begin{cases} K'(l, i, j), & 1 \leq l \leq L' \\ \Phi(0, 0, h_{l-L'}, s_i, t_j) & L' + 1 \leq l \leq L \end{cases}$$

$$f_t(l) = \begin{cases} \delta g(l), & 1 \leq l \leq L' \\ \delta n_0(l - L'), & L' + 1 \leq l \leq L \end{cases}$$

The weight function introduced in (2.21) is taken as

$$P_l = \frac{1 - \mu}{L'}, \quad 1 \leq l \leq L'$$

$$P_l = \frac{\mu \delta^2}{\eta^2 L''}, \quad L' + 1 \leq l \leq L' + L'' = L$$

and the meaning of  $\delta$  remains the same (the rms error of WSBI leading edge).

6. A corrected ionospheric model is formed by replacing

$$u \rightarrow u + \delta u$$

$$n = \hat{N}u$$

7. Ray tracing is used to calculate the new theoretical leading edge  $g(f, \varphi)$  and the optimum elevation angle  $\beta_m(\varphi, f)$  functions for all values of frequency and azimuth at which the experimental leading edge points are specified.

8. The generalized discrepancy is calculated:

$$\rho = (1 - \mu) \|\tilde{g} - g\| + \frac{\mu \delta^2}{\eta^2} \|n(0, 0, h) - n_0(h)\| - \delta^2$$

Iterations are stopped if  $\rho$  and  $\delta u$  are small enough (meaning that the iterative solution has approached the true one) . Otherwise the process returns to the step 4 above.

## 2. Numerical Solution of Two Dimensional Fredholm Integral Equation of the First Kind

### 2.1. General Relationships

Numerical methods for solution of one dimensional (the unknown function is a function of one variable) integral equation of the first kind were described in literature before [Tikhonov and Arsenin, 1977]. My realization of the regularization method for two dimensional (the unknown function is a function of two variables) integral equation of the first kind is described here.

Consider the integral equation

$$f(x, p) = \iint K(x, p, s, t) y(s, t) ds dt, \quad (1)$$

where  $f(x, p)$  and the kernel  $K(x, p, s, t)$  are considered to be known functions. Introduce the regularizing functional

$$\Omega[y] = \iint \left[ y^2 + q_s \left( \frac{\partial y}{\partial s} \right)^2 + q_t \left( \frac{\partial y}{\partial t} \right)^2 \right] w ds dt, \quad (2)$$

where  $q_s(s, t)$ ,  $q_t(s, t)$ , and  $w(s, t)$  are specified positive weight functions. Then the smoothing functional is

$$\begin{aligned} \Phi_\alpha[y] = & \iint \left[ \iint K(x, p, s, t) y(s, t) ds dt - f(x, p) \right]^2 dx dp \\ & + \alpha \iint \left[ y^2 + q_s \left( \frac{\partial y}{\partial s} \right)^2 + q_t \left( \frac{\partial y}{\partial t} \right)^2 \right] w ds dt \end{aligned} \quad (3)$$

Here  $\alpha$  is a positive constant called the regularization parameter. In order to find the  $y$  that minimizes this functional I need to calculate the first variation of the functional. Let us first find variation of the regularizer:

$$\begin{aligned}\delta\Omega &= 2 \iint \left[ y\delta y + q_s \frac{\partial y}{\partial s} \frac{\partial}{\partial s} \delta y + q_t \frac{\partial y}{\partial t} \frac{\partial}{\partial t} \delta y \right] w ds dt \\ &= 2 \iint \left[ y - \frac{\partial}{\partial s} \left( w q_s \frac{\partial y}{\partial s} \right) - \frac{\partial}{\partial t} \left( w q_t \frac{\partial y}{\partial t} \right) \right] \delta y ds dt + 2 \iint \left[ \frac{\partial}{\partial s} \left( \delta y w q_s \frac{\partial y}{\partial s} \right) + \frac{\partial}{\partial t} \left( \delta y w q_t \frac{\partial y}{\partial t} \right) \right] ds dt \\ &= 2 \iint \left[ y - \frac{\partial}{\partial s} \left( w q_s \frac{\partial y}{\partial s} \right) - \frac{\partial}{\partial t} \left( w q_t \frac{\partial y}{\partial t} \right) \right] \delta y ds dt + 2 \oint w \delta y \left( q_s \frac{\partial y}{\partial s} dt - q_t \frac{\partial y}{\partial t} ds \right)\end{aligned}$$

In evaluating this expression the divergence theorem was used.

Now

$$\begin{aligned}\frac{1}{2} \delta\Phi_\alpha &= \iint \left\{ \iint \left[ \iint K(x, p, s', t') y(s', t') ds' dt' - f(x, p) \right] K(x, p, s, t) dx dp \right. \\ &\quad \left. + \alpha \left[ y - \frac{\partial}{\partial s} \left( w q_s \frac{\partial y}{\partial s} \right) - \frac{\partial}{\partial t} \left( w q_t \frac{\partial y}{\partial t} \right) \right] \delta y ds dt + \oint w \delta y \left( q_s \frac{\partial y}{\partial s} dt - q_t \frac{\partial y}{\partial t} ds \right) \right\}\end{aligned}$$

The above expression must be zero at arbitrary  $\delta y$ . Consequently the solution  $y_\alpha(s, t)$  that minimizes (3) at a given  $\alpha$  may be found from the following integro-differential equation (Euler equation):

$$\begin{aligned}\iint G(s, t, s', t') y(s', t') ds' dt' \\ + \alpha \left[ 1 - \frac{\partial}{\partial s} w(s, t) q_s(s, t) \frac{\partial}{\partial s} - \frac{\partial}{\partial t} w(s, t) q_t(s, t) \frac{\partial}{\partial t} \right] y(s, t) = F(s, t)\end{aligned} \tag{4}$$

The equation must be solved with the boundary condition

$$q_s \frac{\partial y}{\partial s} - q_t \frac{\partial y}{\partial t} \frac{ds}{dt} = 0 \quad (\text{along the boundary}) \quad (5)$$

Here

$$G(s, t, s', t') = \iint K(x, p, s, t) K(x, p, s', t') dx dp \quad (6)$$

$$F(s, t) = \iint K(x, p, s, t) f(x, p) dx dp \quad (7)$$

Let  $\delta$  be the *a priori* root-mean-square uncertainty in measuring  $f(x, p)$ , then the following is the regularized formulation of the inverse problem (1):

$$\iint \left[ f(x, p) - \iint K(x, p, s, t) y(s, t) ds dt \right]^2 dx dp \leq \delta^2 \iint dx dp \quad (8)$$

$$\Omega[y] \rightarrow \min \quad (9)$$

Solution of this problem is designed as follows:

If the inequality

$$\iint [f(x, p)]^2 dx dp \leq \delta^2 \iint dx dp \quad (10)$$

holds, then  $y(s, t) = 0$  is the solution of (8), (9). Otherwise the integro-differential equation

(4) is solved with boundary conditions (5) for a set of  $\alpha$  so that a set of solutions

$y_\alpha(s, t)$  is obtained. These solutions are then used to find the so called generalized

discrepancy function

$$\rho(\alpha) = \iint \left[ f(x, p) - \iint K(x, p, s, t) y_\alpha(s, t) ds dt \right]^2 dx dp - \delta^2 \iint dx dp \quad (11)$$

The optimum regularization parameter  $\alpha_d$  is the root of the equation

$$\rho(\alpha_d) = 0 \quad (12)$$

and

$$y(s, t) = y_{\alpha_d}(s, t) \quad (13)$$

is the solution of the regularized problem.

## 2.2. Regularization Method in a Rectangular Region

In the practically important case of rectangular region of integration in (1), that is when the region of integration is determined as

$$\begin{aligned} a &\leq s \leq b \\ c &\leq t \leq d \end{aligned}$$

it is possible to rewrite some of the above relationships in more concrete form. I will write down these relationships for future use in the description of the numerical method.

The range of variables  $x, p$  remains arbitrary.

The source integral equation (1) now is

$$f(x, p) = \int_a^b \int_c^d K(x, p, s, t) y(s, t) ds dt \quad (14)$$

The Euler equation (4) is reformulated as

$$\begin{aligned} &\int_a^b \int_c^d G(s, t, s', t') y(s', t') ds' dt' \\ &+ \alpha \left[ 1 - \frac{\partial}{\partial s} w(s, t) q_s(s, t) \frac{\partial}{\partial s} - \frac{\partial}{\partial t} w(s, t) q_t(s, t) \frac{\partial}{\partial t} \right] y(s, t) = F(s, t) \end{aligned} \quad (15)$$

and its boundary conditions (in accordance with (5)) are:

$$\begin{aligned}
q_s \frac{\partial y}{\partial s} \Big|_{s=a} &= q_s \frac{\partial y}{\partial s} \Big|_{s=b} = 0, \quad c \leq t \leq d \\
q_t \frac{\partial y}{\partial t} \Big|_{t=c} &= q_t \frac{\partial y}{\partial t} \Big|_{t=d} = 0, \quad a \leq s \leq b
\end{aligned} \tag{16}$$

Finally the discrepancy function (11) is rewritten as

$$\rho(\alpha) = \iint \left[ f(x, p) - \int_a^b \int_c^d K(x, p, s, t) y(s, t) ds dt \right]^2 dx dp - \delta^2 \iint dx dp \tag{17}$$

### 2.3. Numerical Realization of the Regularization Method for Two-Dimensional Integral Equation of the First Kind

In order to accomplish the numerical solution, a finite element approximation must be introduced.

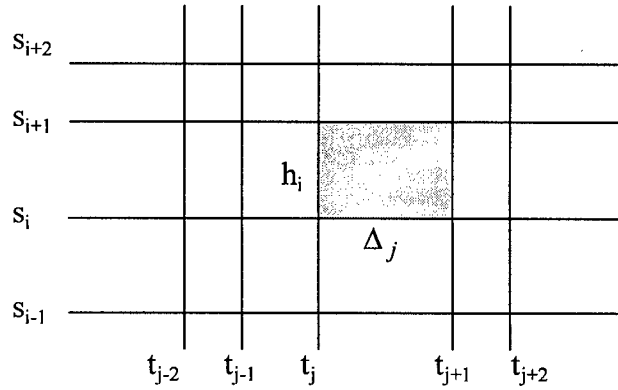


Figure 1. Grid of variables  $s, t$

Let us use the rectangular grid  $s_i, t_j$  (Fig. 1) subject to the following conventions:

$$s_1 = a, \quad s_M = b$$

$$t_1 = c, \quad t_N = d$$

$$1 \leq i \leq M$$

$$1 \leq j \leq N$$

It is possible to conveniently incorporate the boundary conditions by introducing four fictitious grid lines numbered by  $i=-1$ ,  $i=M+1$ ,  $j=-1$ , and  $j=N+1$ . The lines are placed infinitesimally close to the boundary but lie outside the boundary (Figure 2 illustrates how the grid lines  $i=-1$  and  $j=-1$  are introduced).

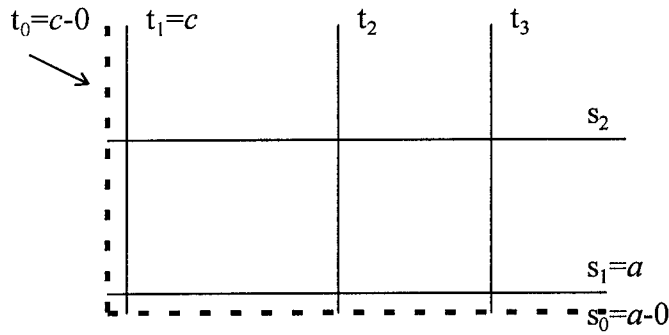


Figure 2. Auxiliary grid lines (the dashed lines) for incorporation of boundary conditions

Then the boundary conditions (16) are equivalent to the relationships:

$$y(0, j) = y(1, j)$$

$$y(M+1, j) = y(M, j), \quad 1 \leq j \leq N$$

$$y(i, 0) = y(i, 1)$$

$$y(i, N+1) = y(i, N), \quad 1 \leq i \leq M$$

All integrals over  $s, t$  are approximated by finite sums as follows:

$$\int_a^b \int_c^d \Psi(s, t) ds dt \approx \sum_{\substack{1 \leq i \leq M \\ 1 \leq j \leq N}} \Psi(s_i, t_j) r_{ij}, \quad (18)$$

where  $r_{ij}$  is a weight function which is specific for each method of numerical integration.

I am using the trapezoid formula, so that

$$r_{ij} = \frac{1}{4} (h_i + h_{i-1}) (\Delta_j + \Delta_{j-1}) \quad (19)$$

where

$$\begin{aligned} h_i &= s_{i+1} - s_i, \quad 1 \leq i \leq M \\ \Delta_j &= t_{j+1} - t_j, \quad 1 \leq j \leq N \end{aligned} \quad (20)$$

Note that effectively in application to the integration formulas (18) and (19) there

$$h_0 = h_M = \Delta_0 = \Delta_N = 0.$$

Now consider approximation of integrals over the variables  $x, p$ . It is more convenient to refrain from specifying any structural detail of the grid for these variables.

Suppose that nodes of this grid are numbered by one integer  $l$ ,

$$1 \leq l \leq L$$

then

$$\iint \Psi(x, p) dx dp \approx \sum_{l=1}^L \Psi(x_l, p_l) P_l. \quad (21)$$

Here  $P_l$  is an appropriate weight function. In order to simplify notations in the discussion of numerical method that follows below I will replace the combination  $x_l, p_l$  by  $l$ :

$$x_l, p_l \rightarrow l.$$

I will use the following replacements as well

$$s_i \rightarrow i$$

$$t_j \rightarrow j$$

Here are the finite dimensional approximations of (5), (6), and (15):

$$G(i, j, i', j') = \sum_{l=1}^L K(l, i, j) K(l, i', j') P_l \quad (22)$$

$$F(i, j) = \sum_{l=1}^L K(l, i, j) f(l) P_l \quad (23)$$

$$\begin{aligned} & \sum_{i', j'} G(i, j, i', j') y(i', j') r_{i'j'} + \alpha w(i, j) y(i, j) \\ & - \frac{2\alpha}{h_i + h_{i-1}} \left\{ \frac{q_s(i+1/2, j) w(i+1/2, j)}{h_i} [y(i+1, j) - y(i, j)] \right. \\ & \quad \left. - \frac{q_s(i-1/2, j) w(i-1/2, j)}{h_{i-1}} [y(i, j) - y(i-1, j)] \right\} \\ & - \frac{2\alpha}{\Delta_j + \Delta_{j-1}} \left\{ \frac{q_t(i, j+1/2) w(i, j+1/2)}{\Delta_j} [y(i, j+1) - y(i, j)] \right. \\ & \quad \left. - \frac{q_t(i, j-1/2) w(i, j-1/2)}{\Delta_{j-1}} [y(i, j) - y(i, j-1)] \right\} \\ & = F(i, j) \end{aligned} \quad (24)$$

It is advisable to multiply (24) by  $r_{ij} / r_0$ , where  $r_0$  is a normalizing constant. This operation will transform (24) into a system of equations with symmetric matrix (the symmetry is with respect to swapping of  $i, j$  with  $i', j'$ , note that matrix  $G$  is symmetric in this sense). The preservation of the symmetry of the matrix is essential for the sake of economizing the use of computer memory. Finally (24) may be rewritten as

$$\sum_{i'=1}^M \sum_{j'=1}^N Z_{ij,i'j'} y(i', j') = F(i, j) r_{ij} / r_0, \quad 1 \leq i \leq M; \quad 1 \leq j \leq N \quad (25)$$

Where

$$Z_{ij,i'j'} = \frac{r_{ij} G(i, j, i', j') r_{i'j'}}{r_0} + \alpha C_{ij,i'j'}$$

Matrix C may be represented in terms of three M by N matrices:

$$C_{ij,i'j'} = C_{ij}^1 \delta_{ii'} \delta_{jj'} + C_{ij}^2 \delta_{ii'+1} \delta_{jj'} + C_{ij}^3 \delta_{ii'} \delta_{jj'+1} + C_{i'j'}^2 \delta_{i+1,i'} \delta_{jj'} + C_{i'j'}^3 \delta_{ii'} \delta_{j+1,j'} \quad (26)$$

Where

$$C_{ij}^2 = -\frac{1}{2} \frac{\Delta_j + \Delta_{j-1}}{r_0 h_{i-1}} w\left(i - \frac{1}{2}, j\right) q_s\left(i - \frac{1}{2}, j\right), \quad \text{at} \quad \begin{array}{l} 2 \leq i \leq M \\ 1 \leq j \leq N \end{array} \quad (27)$$

$$C_{ij}^3 = -\frac{1}{2} \frac{h_i + h_{i-1}}{r_0 \Delta_{j-1}} w\left(i, j - \frac{1}{2}\right) q_t\left(i, j - \frac{1}{2}\right), \quad \text{at} \quad \begin{array}{l} 1 \leq i \leq M \\ 2 \leq j \leq N \end{array} \quad (28)$$

$$C_{ij}^1 = \frac{1}{r_0} r_{ij} w(i, j) - C_{ij}^2 - C_{ij}^3 - C_{ij+1}^3$$

$C_{ij}^2$  and  $C_{ij}^3$  are zero outside the range of indexes indicated in (27), (28). A possible

choice of  $r_0$  is:

$$r_0 = \frac{(b-a)}{M} \frac{(d-c)}{N}$$

Thus, (25) establishes a system of  $M \times N$  linear equations on  $M \times N$  unknowns  $y(i, j)$ . This equation is solved numerically using standard procedure for systems of equations with symmetric matrix. The solution obtained is an approximate solution of the equation (15). A regularized solution is obtained as it is described in Sections 1 and 2

with evident replacements of the integrals by their finite sum approximations (18)-(21) and equation (15) by equation (25).

### 3. Reconstruction of the Ionosphere from WSBI Data Collected by the Virginia

#### OTHR

The Navy OTHR systems are comprised of the surveillance radar itself, a quasi-vertical sounder, and a backscatter sounder. It provides nearly simultaneous measurements of the WSBI and QVI ionograms. The sounder obtains WSBI for eight azimuthal beam directions each separated by  $8^\circ$  (this was changed to  $10^\circ$  in November 1995). The central beam direction of the sounder, or boresight, is at  $175^\circ$ , i.e. almost due south.

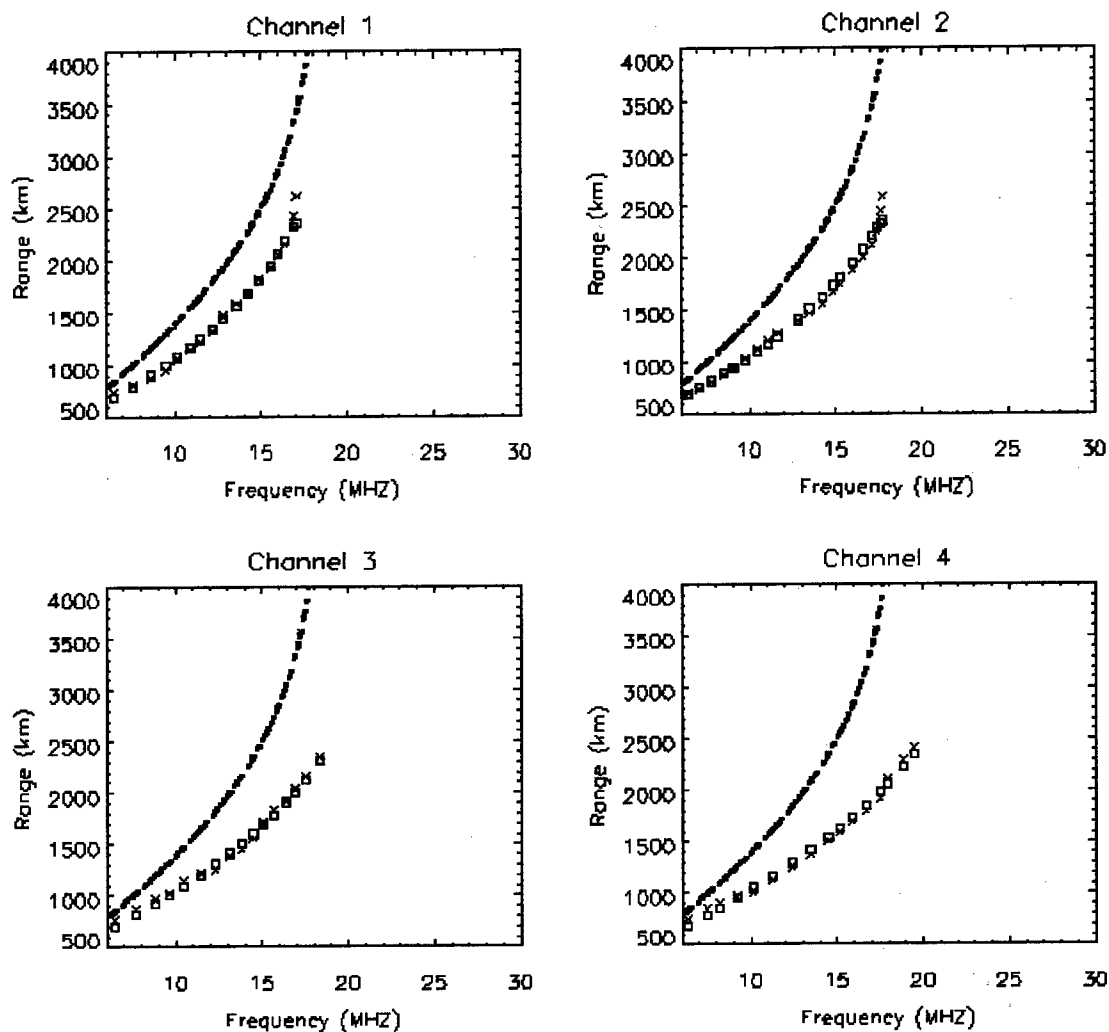
We present here eight examples wherein parameterization (3) was used in each case. This parameterization produces a model that has the same vertical profile shape everywhere, which is not valid for a real ionosphere. Nevertheless, the parameterization has proven to be very useful. It was demonstrated on simulated and real experiments [Fridman and Fridman, 1994, Fridman et al., 1994] that the method produces an accurate reconstruction of horizontal ionospheric variations near the typical altitude of reflection of rays that form the leading edge. In the examples considered here, the reflection points were rather close to the F-region peak (lower by 5 - 25 km) and for that reason we present our inversions in terms of electron density (or plasma frequency) at the altitude of the major maximum of the overhead profile.

Figures 1a, 1b contain eight panels showing, as a function of frequency and delay, the measured (crosses) and iterated (asterisks and squares) leading edges for each of the azimuthal sectors for backscatter soundings acquired on December 8, 1994 starting at 2244 UT (UT is 5 hours ahead of local time). All of the measured data points in these

## Fitting the Leading Edge Data in the 8 Channels

Virginia, December 8, 1994, 22:44 UT

Channels 1 - 4



\*\*\* \*\* theoretical leading edge for the horizontally uniform ionosphere

x x x experimental leading edge points

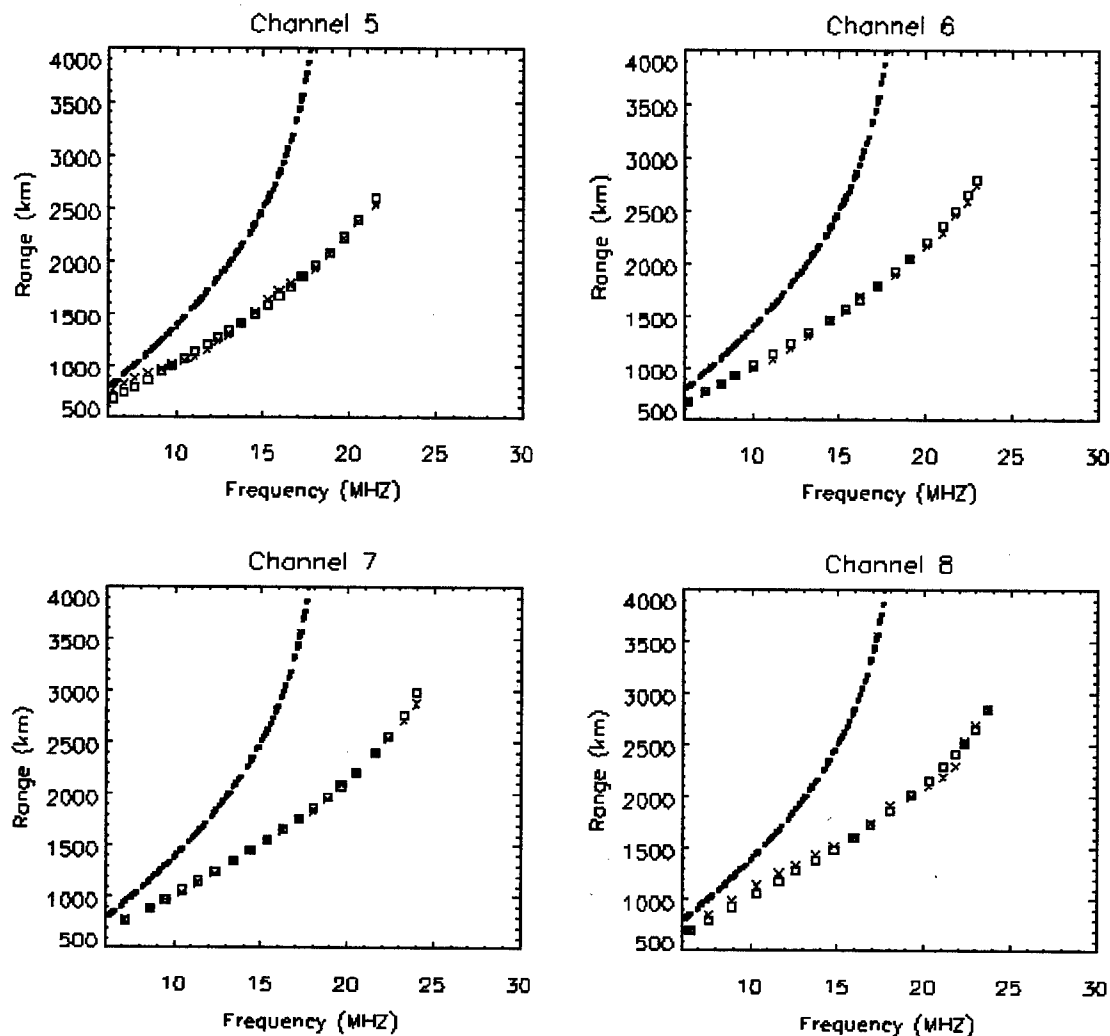
□ □ □ fit by the 3-D inversion technique

Figure 1a

## Fitting the Leading Edge Data in the 8 Channels

Virginia, December 8, 1994, 22:44 UT

Channels 5 - 8



\*\*\* \*\* theoretical leading edge for the horizontally uniform ionosphere

x x x experimental leading edge points

□ □ □ fit by the 3-D inversion technique

Figure 1b

panels were used as input to the WSBI inversion technique; the measurement error for the one way group range was specified as  $\delta = 50$  km. The iterative solution starts from a model that assumes a horizontally uniform ionosphere with the vertical profile being  $n_0(h)$  everywhere. The theoretical leading edge synthesized on the first iteration is shown in Fig. 1 by asterisks; the small squares denote the leading edge for the ionospheric model obtained from the final iteration.

Figure 2 is a contour plot of the reconstructed distribution of plasma frequency at the altitude  $h = 235$  km (i.e. the altitude of the F-layer maximum as obtained by the QVI at the OTHR site) as a function of geographic coordinates. As denoted by the color bar, isolines on this and succeeding figures correspond to integer values of the plasma frequency (in MHz); the red contours show continental and island coastlines. An azimuthal equidistant projection (preserving azimuth and range) from the OTHR was used in creating this contour map and quasi Cartesian coordinates (in km) are also indicated for convenience. The range extent of the area for which the reconstruction is valid is restricted because, at sufficiently large distances, there are no leading edge related rays that pass through the F-region. This restriction was taken into account in determining the greatest range extent of the ionospheric maps presented here.

In this example, acquired near 18h LT, the day-night transition pattern is clearly evident with a relative difference of a factor of two in plasma density across the terminator region. A similar example for data acquired in March 1996 (Fig. 11) exhibits approximately the same difference in density between the sunlit and nightside

### 3-D Inversion of WSBI Leading Edge Virginia, December 8, 1994, 22:44

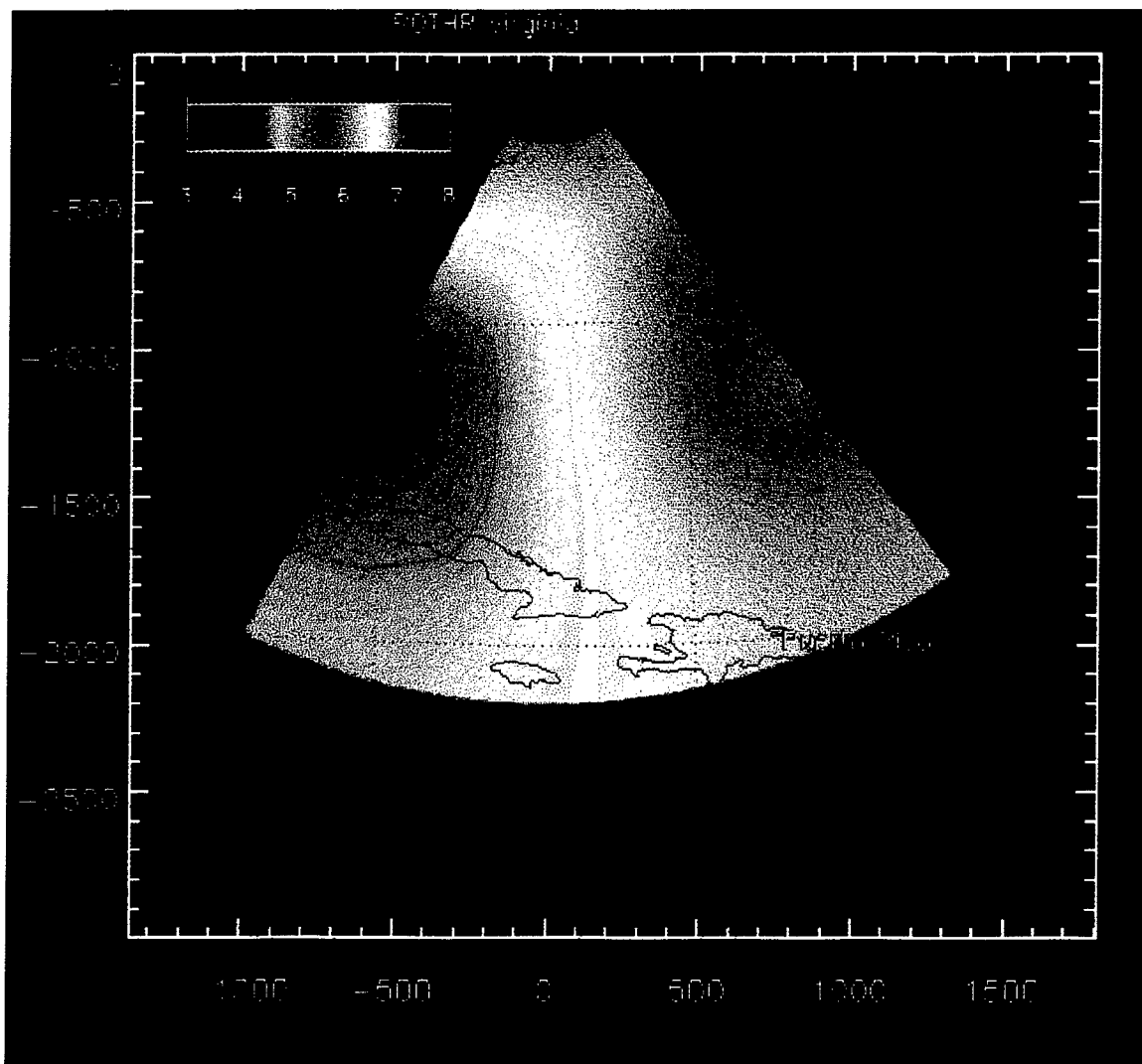


Figure 2. Plasma frequency (MHz) at  $h = 235$  km

ionospheres. These data also show an example of the expanded coverage ( $80^\circ$  sector) that was begun in late 1995 at both OTHR facilities.

The leading edge data shown on Figure 3 demonstrate unusual bending down shape. Inversion of these WSBI's shown on Figure 4 indicates strong latitudinal gradient of plasma density that is perhaps a manifestation of the equatorial anomaly [Kelley, 1989]. This example represents data acquired during the pre-sunset hours in late summer. In the next diagram (Fig. 5), which shows data acquired 1h 48m later, it is evident that the strong gradient had disappeared, with relatively small variations of plasma density that are typical of nighttime conditions.

Data shown in Fig. 6, 7 are characteristic for conditions with negative gradient of electron density typical for pre-midnight time conditions.

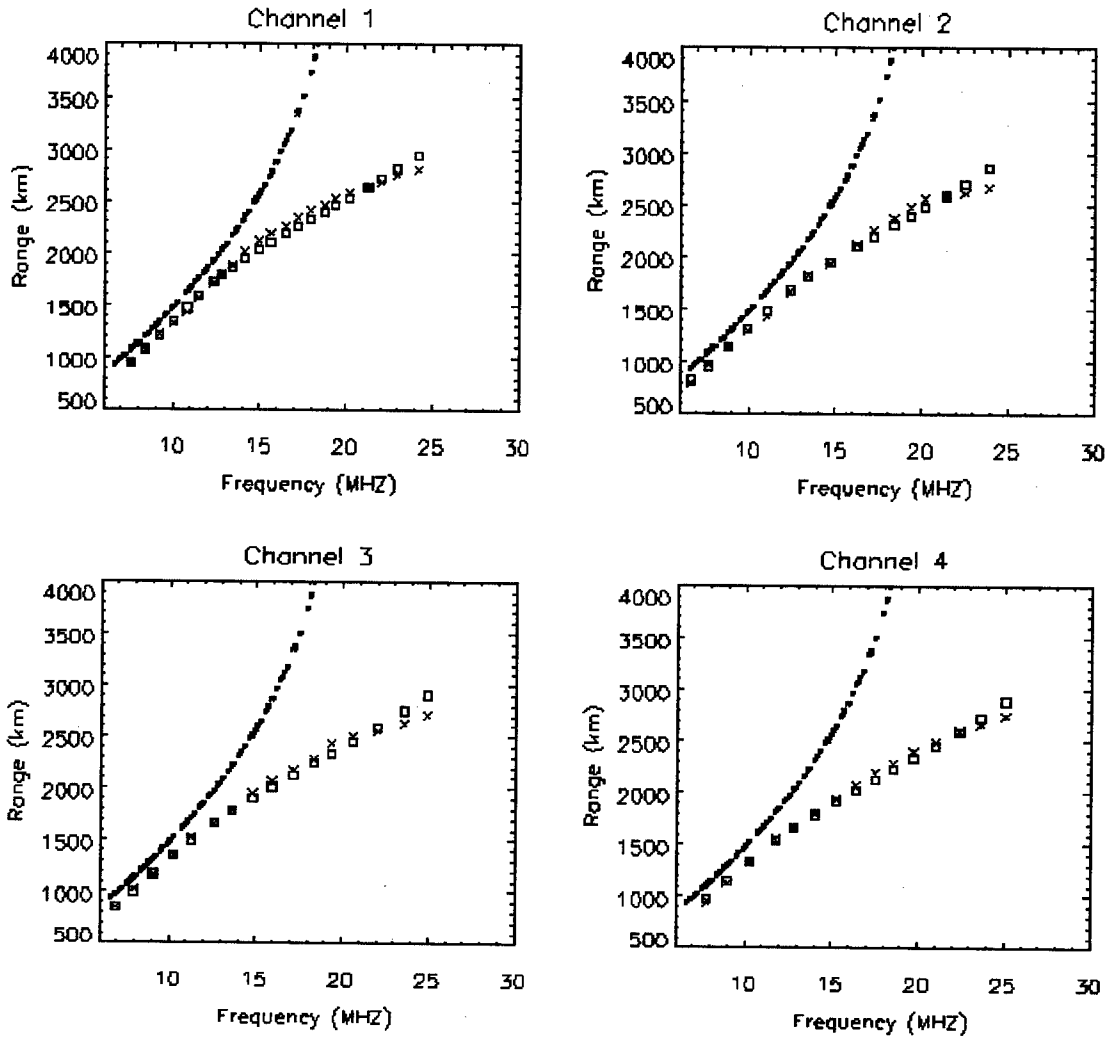
The data shown in Fig. 8 were acquired in the post noon time sector; this case is of interest because the QVI data show evidence of traveling ionospheric disturbances (TIDs) passing overhead, as each successive vertical ionogram was drastically different from the previous one ( $\delta t = 12\text{m}$ ). In general, the reconstructed ionosphere is very smooth and the plasma density varies less than 20%. While it is possible that some features of the weak irregular structure present in Fig. 8 are associated with the TIDs, further observations need to be carried out in order to make a definitive judgment about the effect of TIDs on the large-scale horizontal ionospheric structure.

Figure 9 demonstrates very weak and almost homogeneous ionosphere observed several hours before local sunrise.

## Fitting the Leading Edge Data in the 8 Channels

Virginia, August 5, 1994, 22:57 UT

### Channels 1 - 4



\*\*\* \*\* theoretical leading edge for the horizontally uniform ionosphere

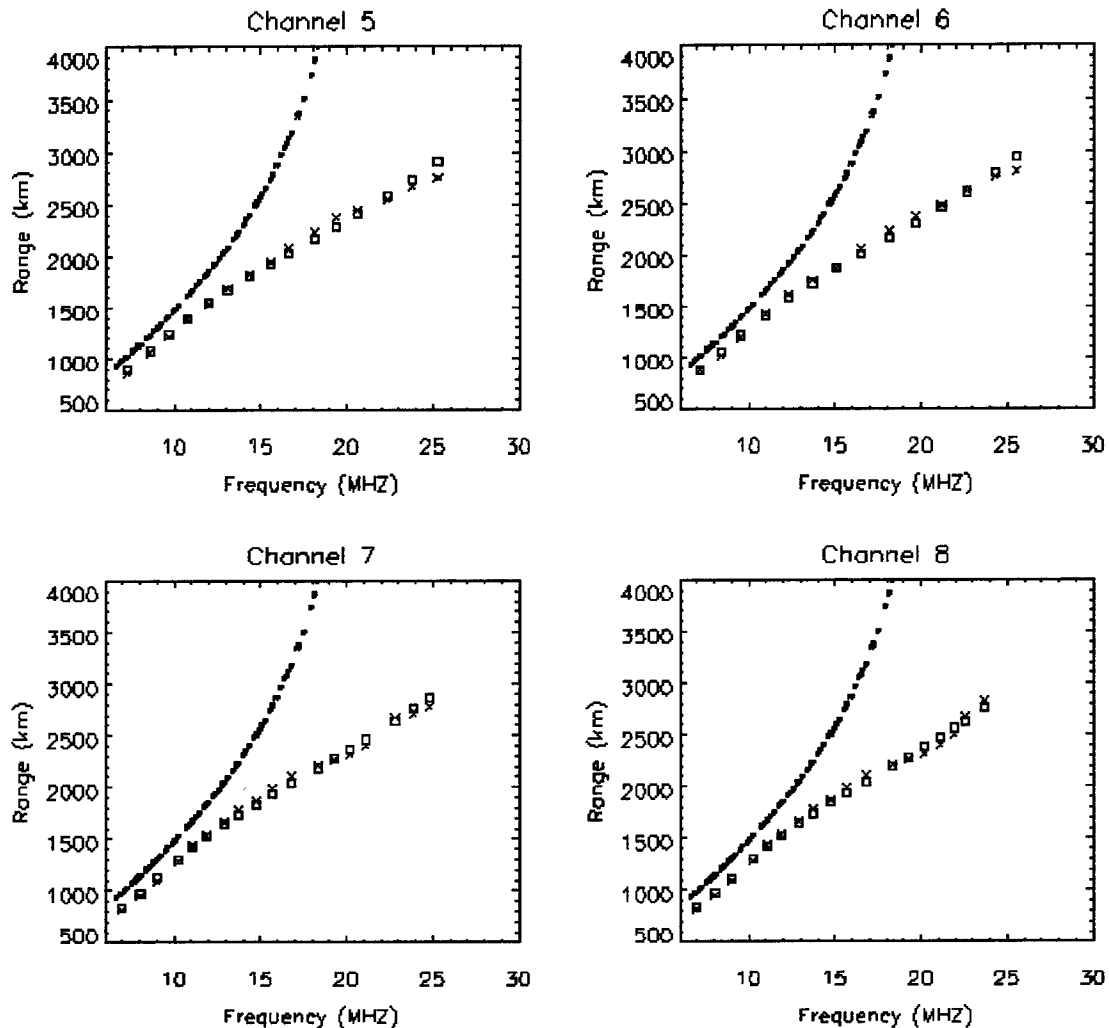
x x x experimental leading edge points

□ □ □ fit by the 3-D inversion technique

Figure 3a

## Fitting the Leading Edge Data in the 8 Channels

Virginia, August 5, 1994, 22:57 UT  
Channels 5 - 8



\*\*\* \*\* theoretical leading edge for the horizontally uniform ionosphere

x x x experimental leading edge points

□ □ □ fit by the 3-D inversion technique

Figure 3b

### 3-D Inversion of WSBI Leading Edge Virginia, August 5, 1994, 22:57

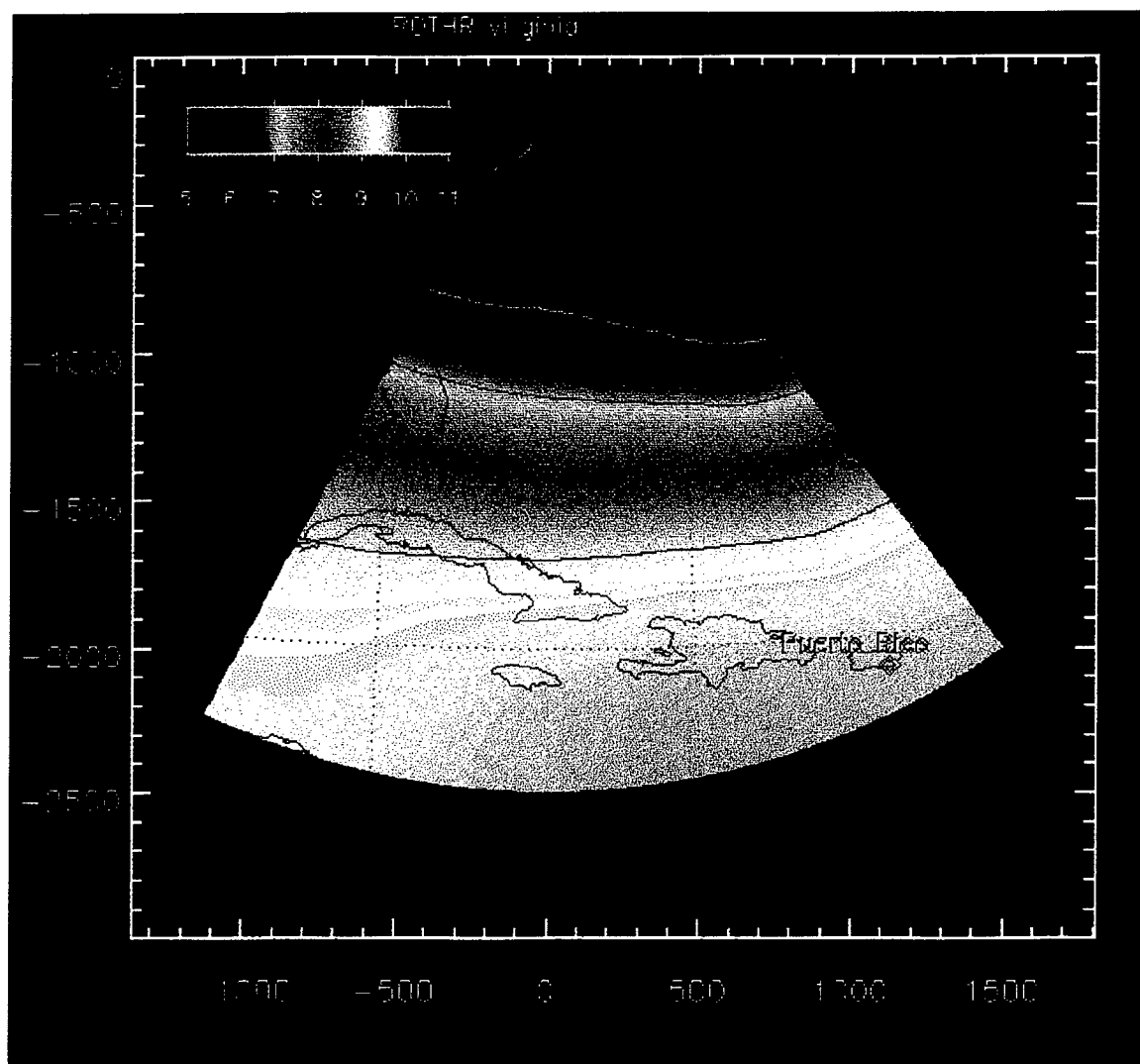


Figure 4. Plasma frequency (MHz) at  $h = 247$  km

### 3-D Inversion of WSBI Leading Edge Virginia, August 6, 1994, 00:45

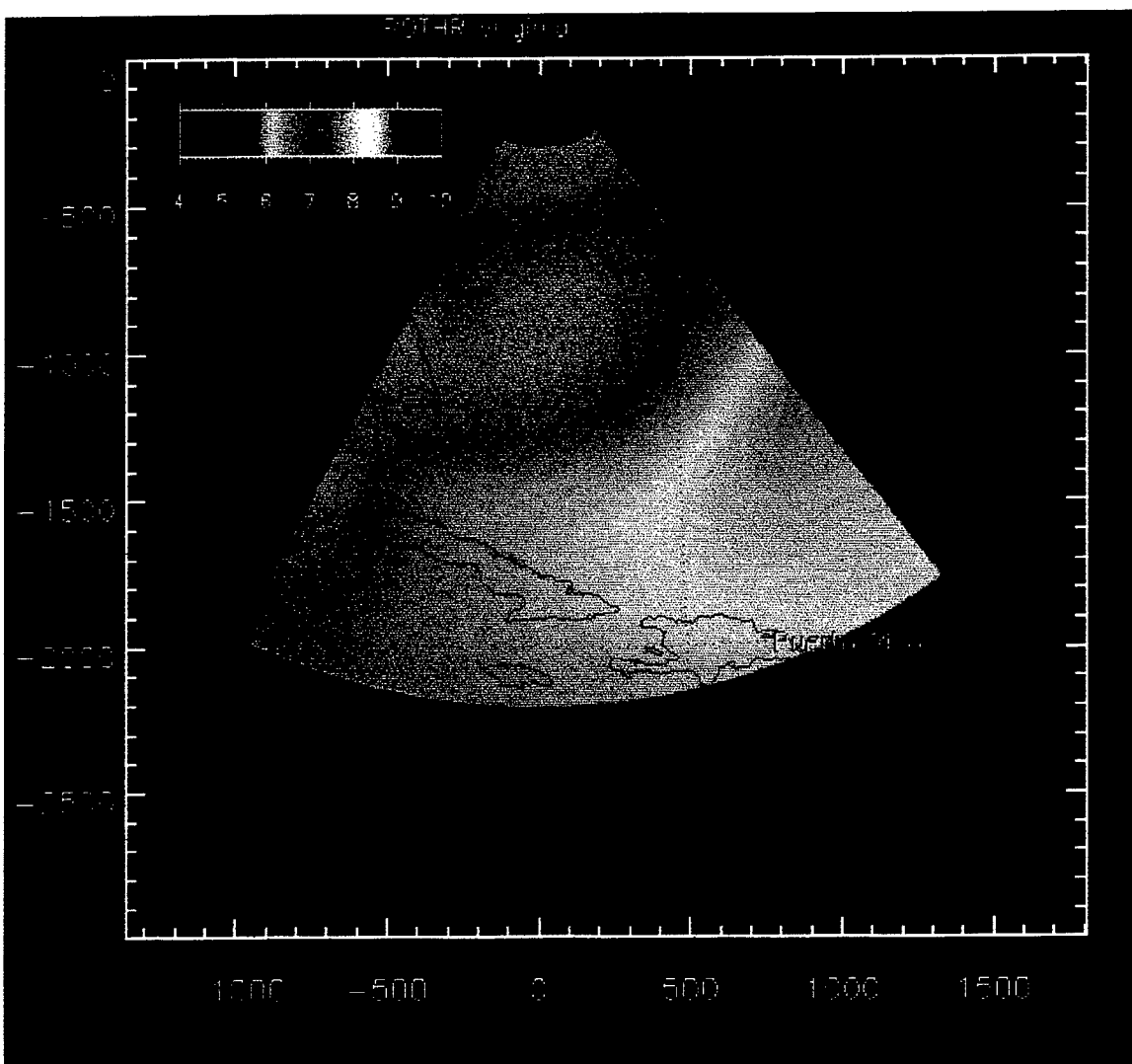
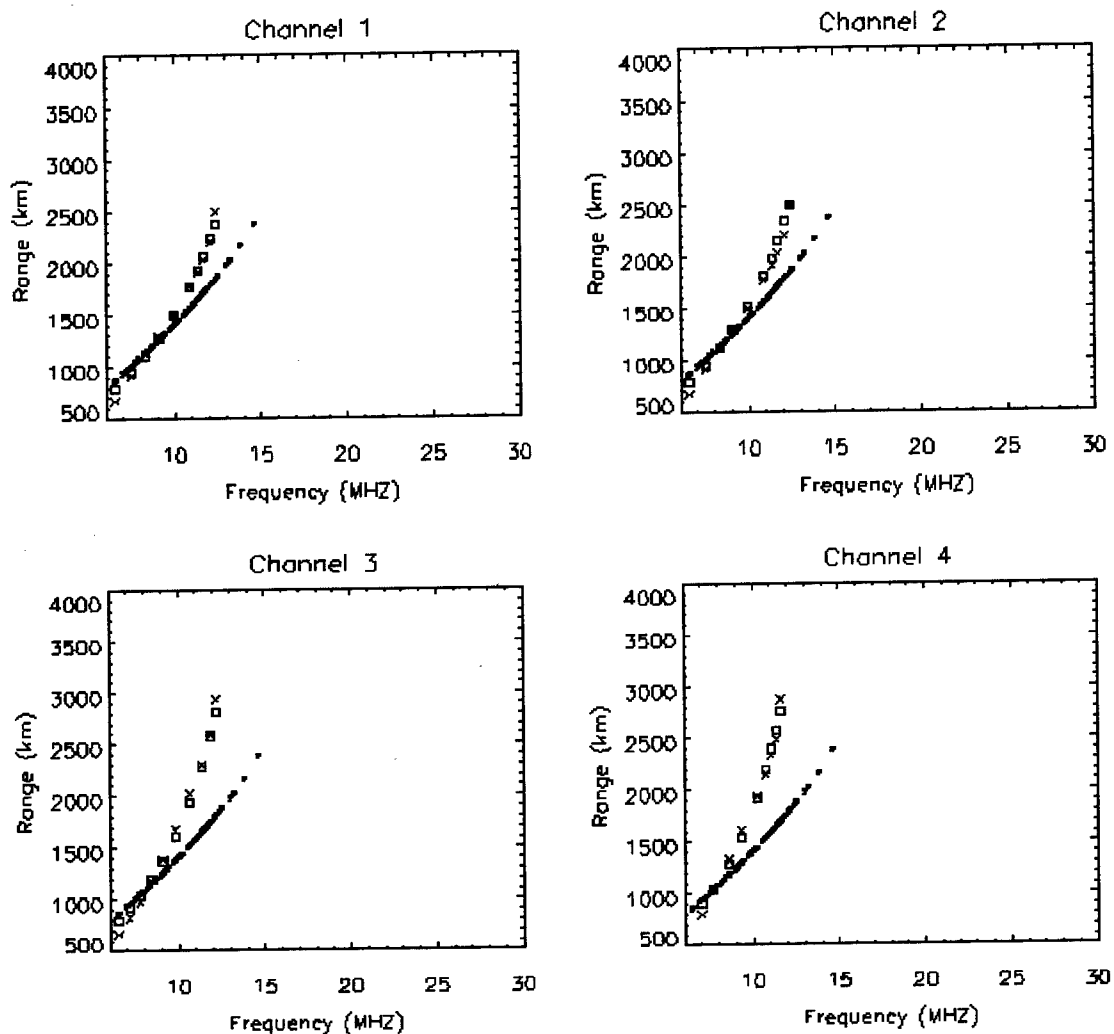


Figure 5. Plasma frequency (MHz) at  $h = 260$  km

## Fitting the Leading Edge Data in the 8 Channels

Virginia, August 6, 1994, 02:21 UT

Channels 1 - 4



\*\*\* \*\* theoretical leading edge for the horizontally uniform ionosphere

x x x experimental leading edge points

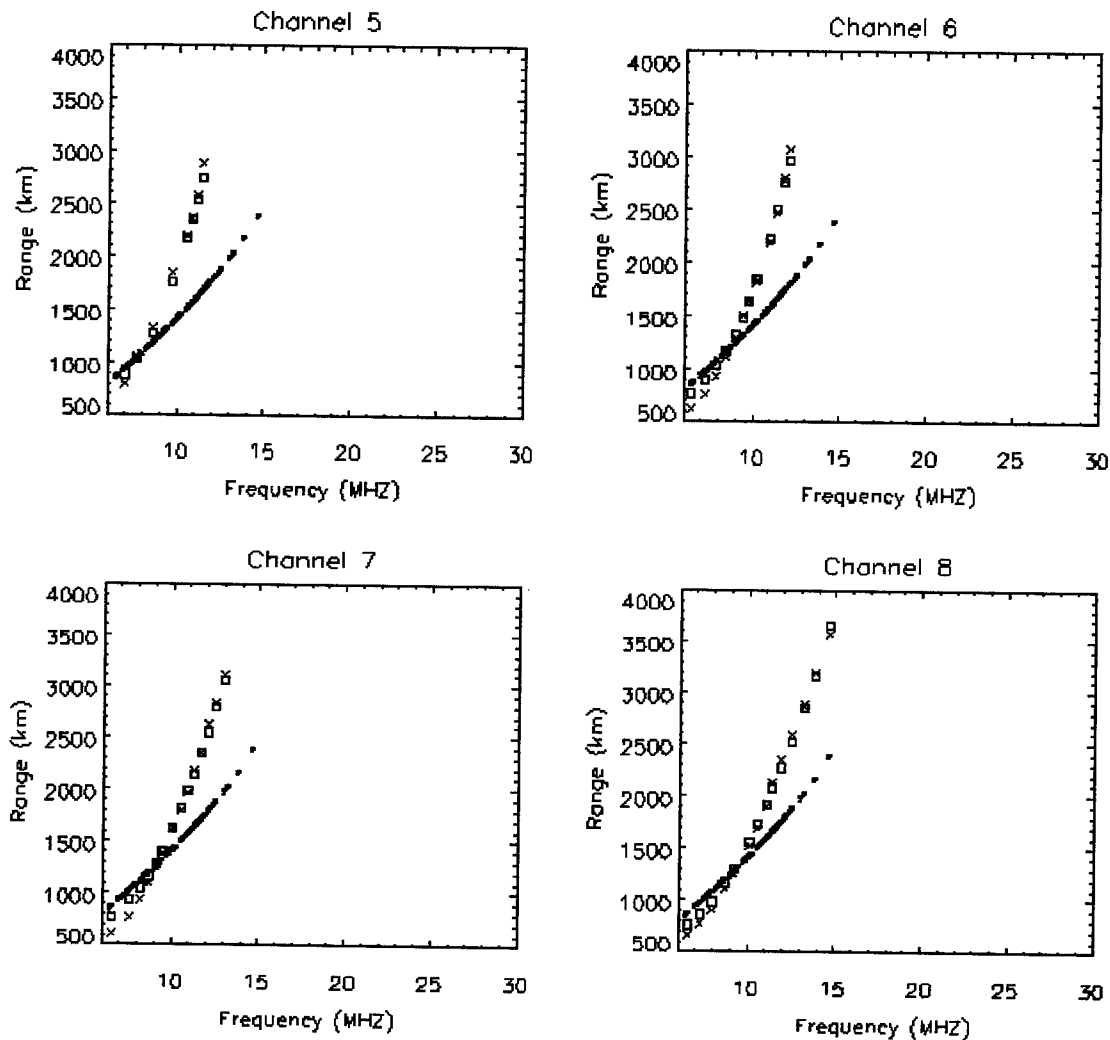
□ □ □ fit by the 3-D inversion technique

Figure 6a

## Fitting the Leading Edge Data in the 8 Channels

Virginia, August 6, 1994, 02:21 UT

Channels 5 - 8



\*\*\* \*\* theoretical leading edge for the horizontally uniform ionosphere

x x x experimental leading edge points

□ □ □ fit by the 3-D inversion technique

Figure 6b

### 3-D Inversion of WSBI Leading Edge Virginia, August 6, 1994, 02:21

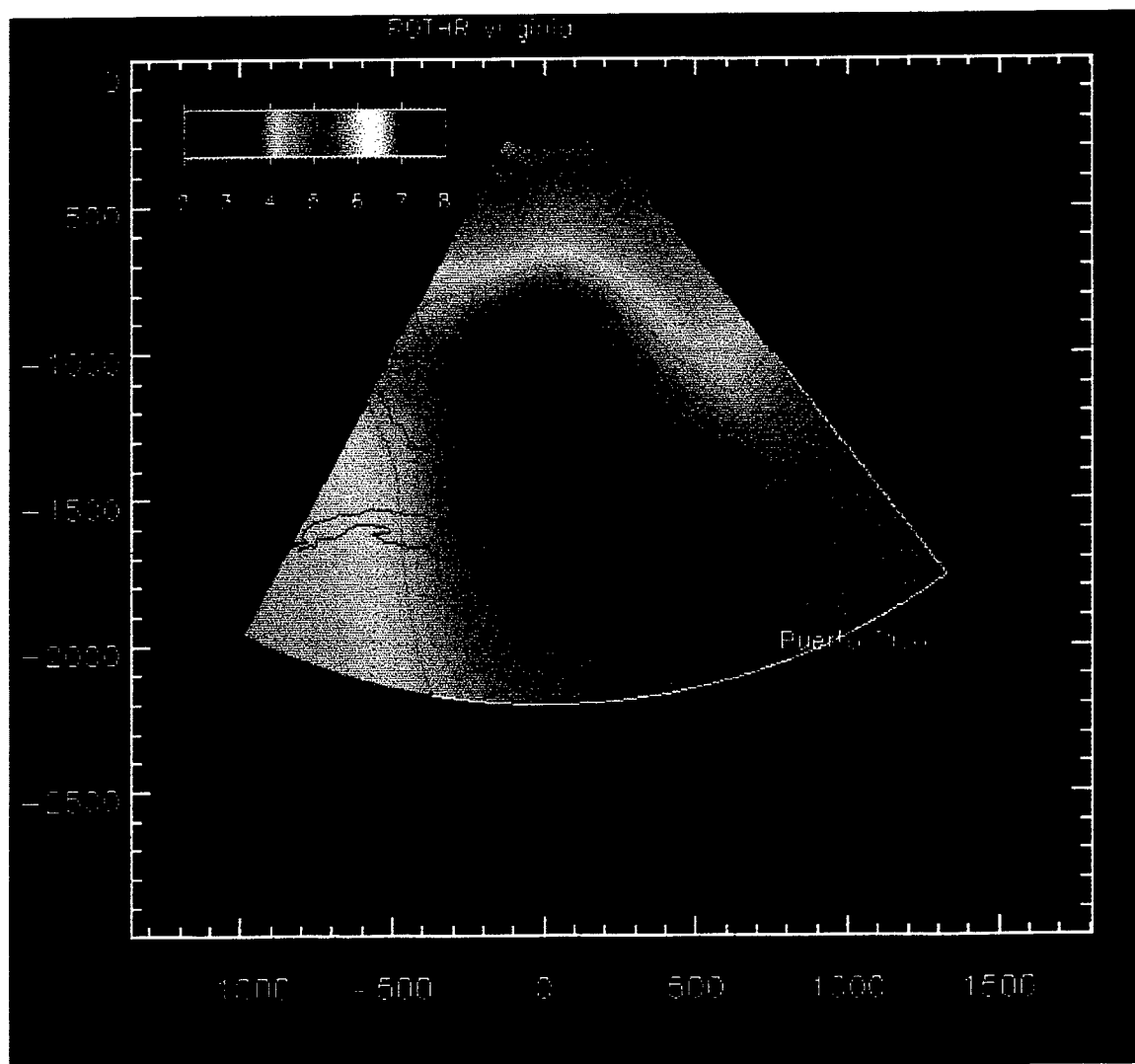


Figure 7. Plasma frequency (MHz) at  $h = 243$  km

### 3-D Inversion of WSBI Leading Edge Virginia, December 7, 1994, 18:50

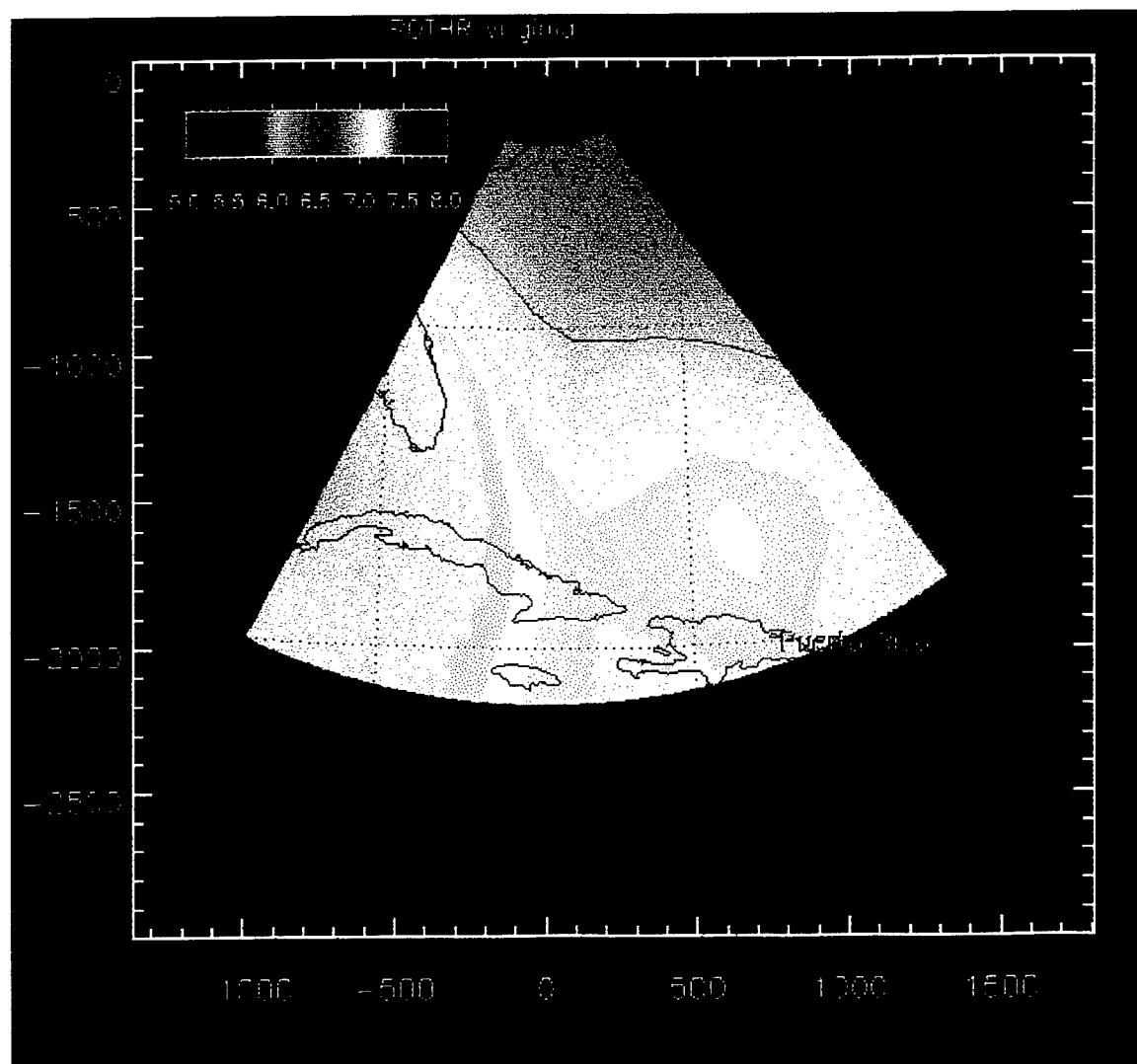


Figure 8. Plasma frequency (MHz) at  $h = 226$  km

### 3-D Inversion of WSBI Leading Edge Virginia, December 8, 1994, 09:05

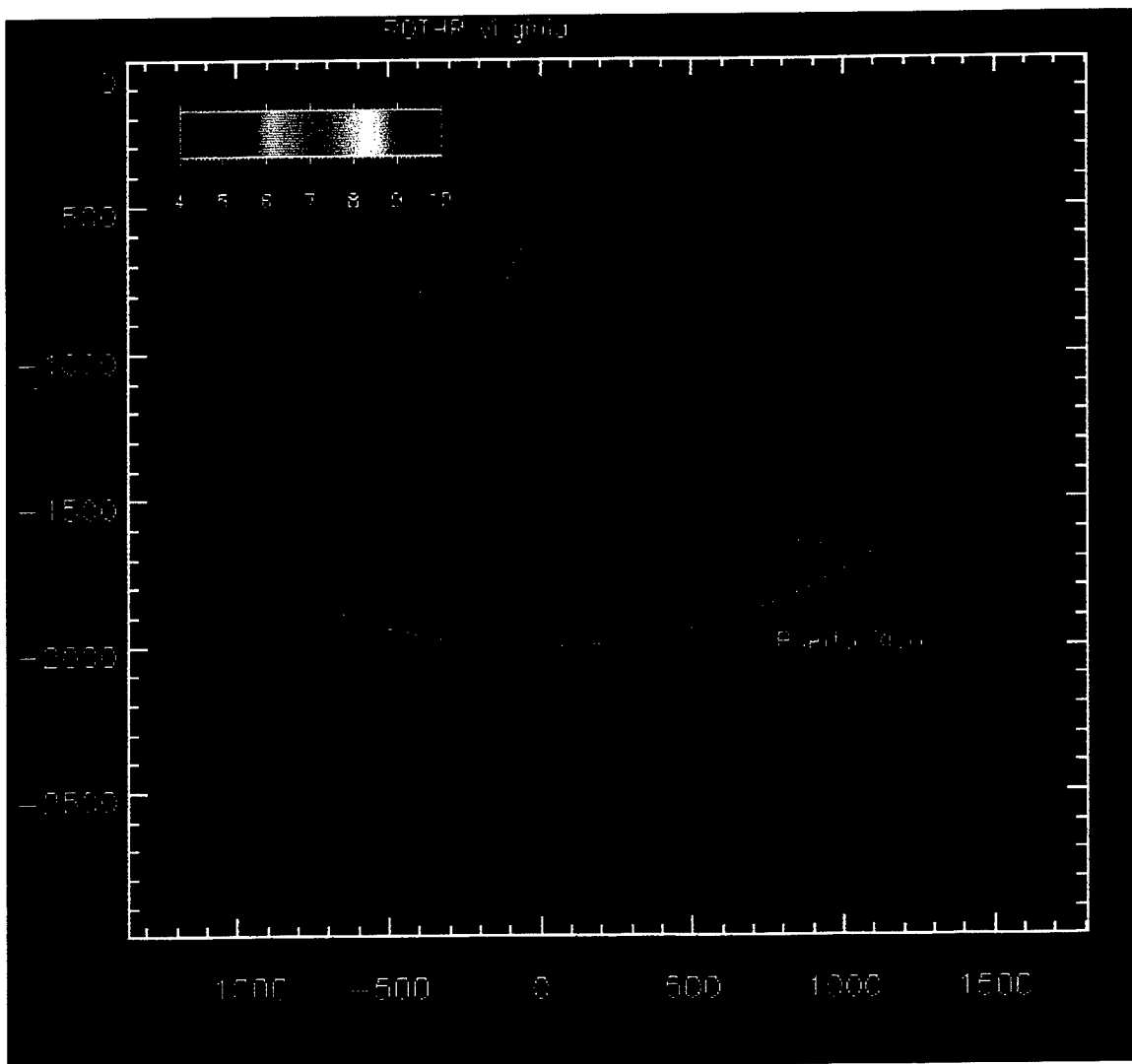


Figure 9. Plasma frequency (MHz) at  $h = 293$  km

Figure 10 shows ionosphere in local noon time. The ionosphere is weakly inhomogeneous at that time.

#### **4. Discussion and Conclusions**

We have demonstrated here the capabilities of the WSBI inversion method as a viable diagnostic tool for determining the spatial variation of medium and large-scale structures in the ionosphere. It is particularly valuable that the method is able to produce two-dimensional snapshots of horizontal structure of the lower F2 region (when the parametrization (3) is used). For the Virginia OTHR these snapshots cover a 64° sector of up to 2000 km radius. None of other extant experimental techniques (e.g. incoherent scatter and ionospheric tomography) employed for ionospheric measurements are capable of providing such a comprehensive picture of the horizontal structure of the ionosphere.

The accuracy of this method has been tested using both simulations and experimental tests [Fridman and Fridman, 1994; Fridman *et al.*, 1994], which show that it provides accurate profiles of the F region below the F2 peak. For other ionospheric layers the diagnostics may not be so effective and to further improve this method, it may be necessary to distinguish between leading edges associated with the E- and F-layers.

Currently there are two OTHRs operating in the US, one in Virginia and another in Texas, making WSBI and QVI ionospheric soundings every 12 minutes. Using available computational resources, the WSBI inversion technique described here is able to perform inversions within the operational cycle of the sounders. Thus, implementation of the WSBI inversion technique at the existing OTHR sites can provide real-time

### 3-D Inversion of WSBI Leading Edge Virginia, March 21, 1996, 17:45

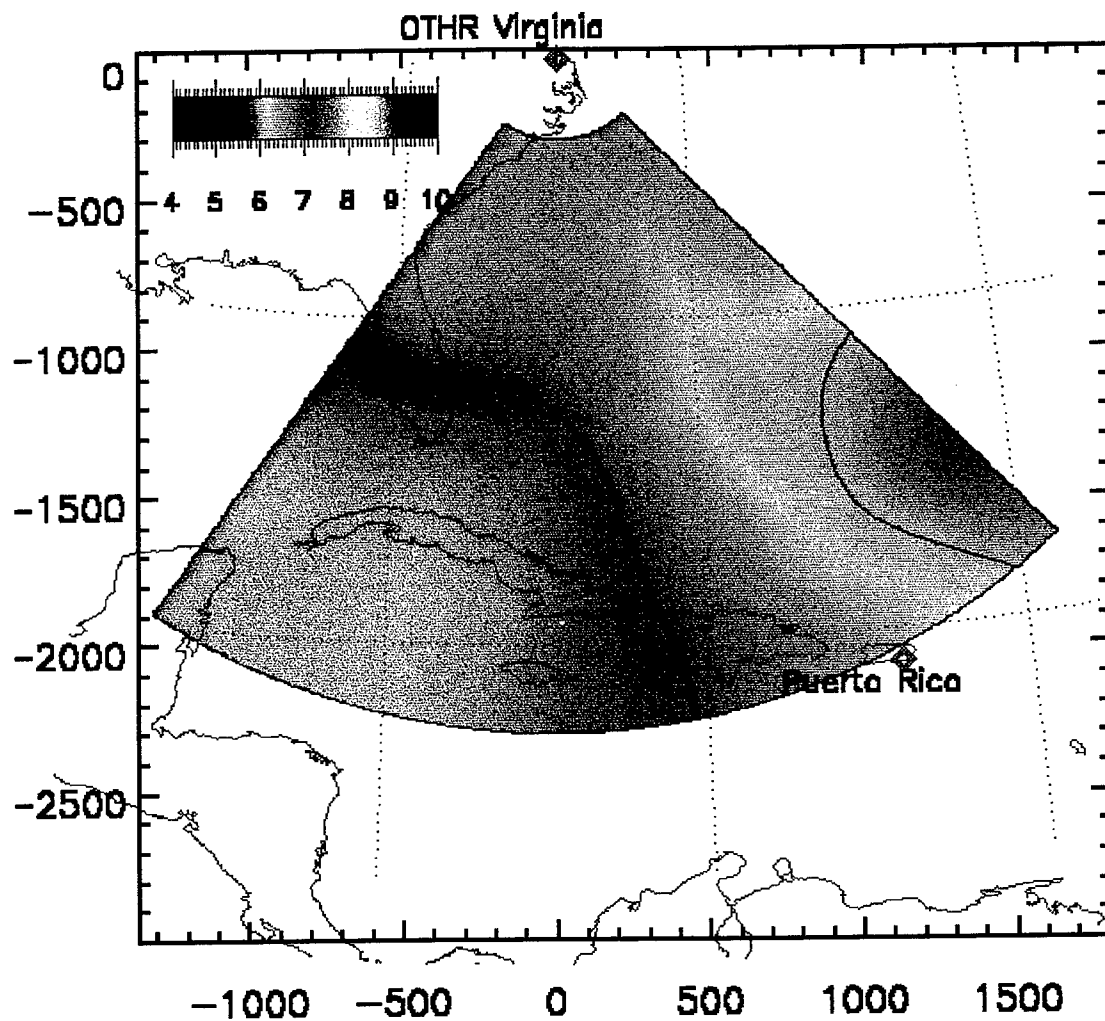


Figure 10. Plasma frequency (MHz) at  $h = 227$  km

### 3-D Inversion of WSBI Leading Edge Virginia, March 21, 1996, 23:09

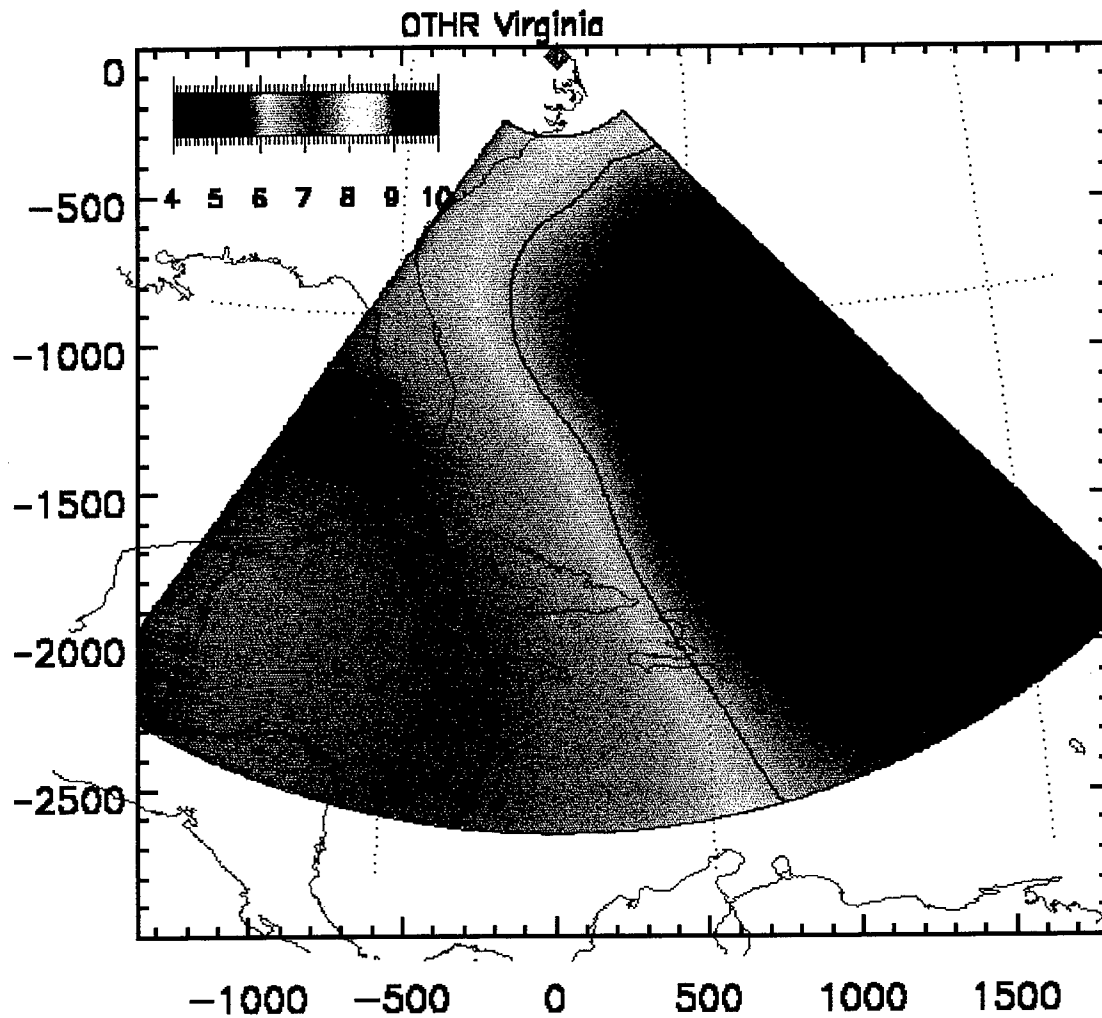


Figure 11. Plasma frequency (MHz) at  $h = 244$  km

monitoring of ionospheric irregularity structures over a very large geographic area. In addition to direct utilization in the OTHR coordinate registration process, this unique information is of potential use to other users of ionospheric propagation information, as well as providing a valuable input to the National Space Weather Program [Wright, 1995, 1997]. Furthermore, routine analysis of this information holds the promise of extending our understanding of the structure and dynamics of medium and large-scale ionospheric irregularities.

Unfortunately this project was terminated two months earlier than planned and we were unable to finish the work on WSBI inversion from simultaneous data of both backscatter sounders. This development was stopped on the debugging stage. If accomplished it could provide enhanced BI inversions for the overlapping coverage region of the two sounders.

**Acknowledgments:** We are grateful to L. J. Nickisch and M. Hausman of Mission Research Corporation for providing us the data and for productive discussions. The extraction of WSBI leading edges and inversion of QVIs was performed by M. Hausman.

## References

- Croft, T.A., Sky-wave backscatter: A means for observing our environment at great distances, *Rev. Geophys. Space Phys.*, **10**, 1972.
- Davies, K. Ionospheric Radio, Peter Peregrinus, Ltd., London, 1990.
- Fridman, O. V., V. E. Nosov, O. N. Boitman, Reconstruction of horizontally inhomogeneous ionospheric structure from oblique-incidence backscatter experiments, *J. Atmos. Terr. Phys.*, **56**(3), 369-376, 1994.
- Fridman, O. V., and S. V. Fridman, A method of determining horizontal structure of the ionosphere from backscatter ionograms, *J. Atmos. Terr. Phys.*, **56**(1), 115-131, 1994.
- Hartsfield, W. L., S. M. Ostrow, and R. Silberstein, Backscatter observations by the Central Radio Propagation Laboratory, August 1947 to March 1948, *J. Res. NBS*, **44**, 199-214, 1950.
- Headrick, J.M., Looking over the horizon, *IEEE Spectrum*, 36-39, July 1990.
- Headrick, J.M. and M.I. Skolnik, Over-the-horizon radar in the HF band, *Proc. IEEE*, **62**, 664-673, 1974.
- Kelley, M. C., The Earth's Ionosphere : Plasma Physics and Electrodynamics, San Diego, Academic Press, 1989.
- Kolmogorov, A. N., and S. V. Fomin, Introductory Real Analysis, New York, Dover Publications, 1975.
- Tikhonov, A. N., V. Y. Arsenin, Solutions of Ill-posed Problems, Washington: Winston; NY, 1977.
- Wright, J.M. Jr., National Space Weather Program, Strategic Plan, FCM-P30-1995, Washington, DC, August 1995.